

e-HIGHWAY 2050

Modular Development Plan of the Pan-European Transmission System 2050

| | | | |
|------------------------|---|-------------------|-----------------------|
| Contract number | 308908 | Instrument | Collaborative Project |
| Start date | 1st of September 2012 | Duration | 40 months |
| WP 8 | Enhanced Pan-European Transmission Planning Methodology | | |
| D8.6a | Detailed enhanced methodology for long-term grid planning | | |



| | | Date & Visa |
|--------------|--|-------------|
| Written by | Camille Pache, Baptiste Seguinot, RTE Sara Lumbreras, Fernando Bañez-Chicharro, Francisco Echavarren, Lukas Sigrist, COMILLAS | 06/11/2015 |
| Checked by | Patrick Panciatici, RTE | 08/11/2015 |
| Validated by | Gérald Sanchis, Nathalie Grisey, RTE | 30/11/2015 |

| | | |
|---|---|---|
| Project co-funded by the European Commission within the Seventh Framework Programme | | |
| Dissemination Level | | |
| PU | Public | X |
| PP | Restricted to other programme participants (including the Commission Services) | |
| RE | Restricted to a group specified by the consortium (including the Commission Services) | |
| CO | Confidential, only for members of the consortium (including the Commission Services) | |

Document information

General purpose

This document is the deliverable D8.6a of the e-Highway2050 project [3]. It contains the description of the enhanced methodology developed in the framework of Work Package 8, and illustrated through a test case. The feasibility of the methodology presented in the previous deliverables was tested in Task 8.6 “Enhanced methodology for long-term planning and specification of the associated tools”. The results from this test case are presented in this document.

This deliverable:

- describes the method which has been developed and prototyped in the framework of this Work Package, and
- illustrates the methodology through a test case of the size of the European system.

Change status

| Revision | Date | Changes description | Authors |
|----------|------------|---------------------------------------|----------------------------------|
| V1.0 | 05/11/2015 | Initial version | C. Pache, B. Seguinot |
| V1.1 | 06/11/2015 | Initial version + Nodal expansion | F. Bañez-Chicharro, S. Lumbreras |
| V1.2 | 06/11/2015 | Initial version + Robustness analysis | F. Echavarren, L. Sigrist |
| V2.0 | 30/11/2015 | Update of nodal expansion results | F. Bañez-Chicharro |
| V2.1 | 30/11/2015 | Updates following review by partners | C. Pache |

EXECUTIVE SUMMARY

Long-term transmission planning over large power systems, such as the European transmission network, is a very large and complex problem. Indeed, transmission planning is usually performed for time horizons comprised between 10 and 20 years and current methods have not coped so far with planning over large areas and with increased uncertainty when integrating significant shares of renewable generation. Several studies are conducted on these topics [15]-[19]. Today, any national transmission system in Europe is planned using expert judgement. Therefore, Work Package 8 of the e-Highway2050 project [3] aims at defining a new methodology where long-term planning is formalised as an optimisation problem, and at specifying new tools. Advanced optimisation and simulation methods are investigated to tackle this complex highly combinatorial problem, taking into account the stochastic and dynamic behaviours of the system. A Monte-Carlo approach has been retained to consider the stochasticity of the problem. The problem is solved from a transmission operator perspective, with no control over generation planning. Though, several possible evolutions of the electricity sector are investigated for different *scenarios*. The main challenges arise from the spatial, temporal and stochastic complexities. Thus, methods to reduce the size of the grid or to choose relevant snapshots among the 8760 hours of a year have been developed. The process followed by the developed methodology is represented in Figure 1.

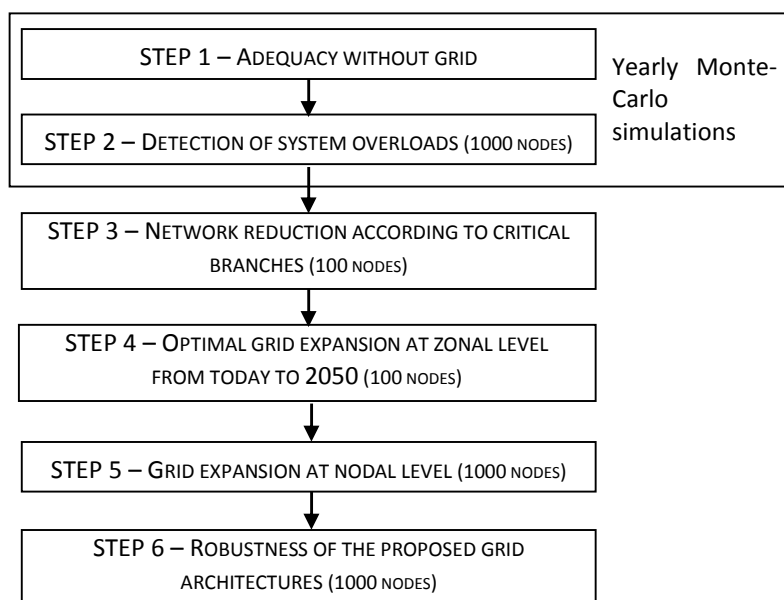


Figure 1 – Methodology proposed in e-Highway2050, WP8

In a first step, controllable generation and consumption are calculated with an hourly time step to ensure power adequacy between production and load for each scenario (i.e. generation mix) and time horizon. Grid constraints are not taken into account at this step and several patterns of uncertainties are considered. In a second step, overload problems are detected on a simplified initial pan-European nodal grid (around 1,000 nodes). Then, in a third step, the initial network is reduced according to critical branches, leading to a zonal initial grid (100 nodes). In a fourth step, the modular development plan is calculated at the zonal level considering all time horizons and the whole set of scenarios. Starting from the zonal modular development plans, a grid expansion is performed for the first two time horizons at a nodal level. Finally, the robustness of the nodal grid architectures is checked to ensure that these grids can be operated without major voltage or stability issues.

This document presents the main aspects of the complete methodology, which was detailed in deliverables 8.2 to 8.5. It is illustrated through a final test case of the size of the European network to test the feasibility

of such long-term grid study and assess the resources that would be needed to perform it. As a reminder, the purpose of this work package is not to perform a real study, such as WP2/WP4. The data used in this test case is not exact, but tries to be realistic in order to check the feasibility of the methodology on a system of the size of the European network.

The final test case is described in the first section. The studied system is based on a large part of the 2012 HV European system, so that it is close to the size of the European network ($\approx 5,000$ nodes). Starting from the 2012 installed capacities and energy mix in the different countries, three contrasted scenarios were built for each of the three considered time horizons (2030, 2040 and 2050). Then, the initial network was reduced to around 1,000 nodes, which is the most detailed grid model used in the methodology.

The generation of production and consumption time series is presented in Section 2. A Monte-Carlo approach has been retained to take into account the stochasticity of the problem and to study the response of the power system to diverse possible events. Thus, time series of RES generation (wind and solar), load, hydro inflows and outages of the generating units are generated for several Monte-Carlo. This is followed by adequacy simulations which are performed on each set of stochastic inputs randomly sampled (i.e. Monte-Carlo year). In the test case, 100 Monte-Carlo years are run for each scenario and each time horizon, leading to 900 simulated years. The importance of considering spatial correlations in adequacy simulations or the impact of Demand Response is illustrated in the test case.

Once the optimal dispatch of generation has been obtained in a copper plate system for the different Monte-Carlo years, and for each scenario and time horizon, we want to quantify the congestion of transmission lines in the initial grid that would be induced by these injections: this is the topic of Section 3. This is done running hourly DC Optimal Power Flows (OPF) which minimize the cost of adjusting controllable generation and load from the optimal dispatch, while complying with network constraints and using in the best way network controls (HVDC lines, Phase Shifter Transformers (PST)). This will enable to detect which lines are the most critical for the system across all the Monte-Carlo years, scenarios and time horizons.

In Section 4, the initial nodal network is reduced to around 100 zones. This network reduction is performed according to critical branches, which should minimize the need for internal reinforcements. Critical lines are either selected using the indicators provided by the DCOPFs, or correspond to power flow control devices (HVDC lines or PST). Once the network partition is obtained, equivalent network characteristics (reactances and capacities) are computed. This zonal model will constitute the starting point for a modular network development plan. The different selection criteria are analysed in the test case and the resulting critical branches and reduced zonal network are presented in this section as well.

The purpose of Transmission Expansion Planning (TEP) is to provide grid expansion candidates that will allow the grid to take advantage of most of the generating units while reducing the load curtailments at a minimal investment cost. It is a trade-off between minimizing the investment costs and minimizing the generation and load curtailment costs. Before optimizing the TEP, two components must be defined: the transmission lines in which the model is allowed to invest, called candidates, and the snapshots on which the impacts on system operation are assessed. These snapshots should represent the whole pool of grid simulations (not only critical situations) so that operational expenses can be estimated. The method we developed, based on a clustering algorithm, is presented in Section 5, as well as the candidate selection and the TEP optimization problem. In the test case, we used nodal price differences as clustering feature for the snapshot selection, however other indicators could be studied. 5 snapshots were selected for each scenario and time horizon, meaning that we selected 5 hours to represent 100 Monte-Carlo years (876,000 hours). This limitation on the number of snapshots arises from the TEP optimization, which was taking too much time with more snapshots. The impact of the number of selected snapshots on the transmission expansion results could also be studied if improvements in the TEP optimization problem are reached. Then, candidates are selected by sorting the feasible and profitable candidates out of the initial pool. This lead to 55 candidates instead of the 9900 possible candidates if all the pairs of zones are considered with two possible types (AC or DC). Finally,

a TEP optimization problem is solved for the zonal network over all the time horizons and scenarios at the same time, with a common development to all scenarios imposed at the first time horizon (2030). Several solver options were tested to improve the performance of this complex mixed integer linear optimization problem. The obtained results are presented at the end of this section.

The expansion at zonal level gives a solution in the form of equivalent physical capacities and reactances between zones for each scenario and time horizon. This is not a directly implementable expansion plan, which needs specific transmission lines with their corresponding end nodes, voltage levels and cable types. Therefore, Section 0 presents the method which computes the nodal plan for the first time horizons (e.g. 2030 in the test case), for which there is a common zonal expansion plan for all the scenarios. First, the most relevant transmission lines that will be considered candidates in the expansion are identified with a similar method than for the zonal expansion. Then, the nodal transmission expansion planning problem to select the optimal lines, taking into account investment and operation costs, is solved using TEPES (Transmission Expansion Planning for an Electrical System), a model developed by Comillas. We should note that the inter-zonal capacities resulting from the zonal development plan for the first time horizons are the only information kept in the nodal expansion. These values are put as constraints in the nodal expansion optimization problem. The obtained nodal expansion plans should ensure system reliability (N-1) taking into account all possible flexible devices, while N-1 contingencies were not considered in the former steps.

Sanity checks to assess the robustness of the proposed nodal grid architectures are proposed in Section 0. The robustness analysis involves the study of voltage-reactive power control and stability, transient stability and small-signal stability. One main output of this task is the development of an algorithm which builds an AC load flow model from a DC one, and ensures its convergence. Indeed, an AC load flow model of the grid is needed to account for reactive power flows and bus voltage magnitude variation. The performance of this method is presented for different test cases in this section. The small-signal stability analysis which was not presented in deliverable D8.5a (“Enhanced methodology to assess robustness of a grid architecture” [9]) relative to this task is detailed in this part, and illustrated with test cases results.

Finally, the last section gathers the main test case results, with a focus on computation times and required resources to run this kind of long-term planning study. It concludes this report with the difficulties we faced running this test case and gives preliminary recommendations for further work. Another deliverable (D8.7 “Recommendations about critical aspects in long-term planning methodologies” [24]) is dedicated to the main conclusions of the work performed in WP8: how existing tools and methods could be improved, what would be the specifications for new tools and recommendations for more research.

TABLE OF CONTENTS

| | |
|--|------------|
| Document information | ii |
| EXECUTIVE SUMMARY | iii |
| TABLE OF CONTENTS | vi |
| List of Figures | 8 |
| List of Tables | 10 |
| 1. Test case description | 11 |
| 1.1. INPUT DATA: INITIAL NETWORK AND ENERGY SCENARIOS | 11 |
| 1.2. INITIAL NETWORK REDUCTION: NODAL NETWORK | 13 |
| 2. Generation of production and consumption scenarios | 15 |
| 2.1. MAINTENANCE SCHEDULING | 15 |
| 2.2. GENERATION OF TIME SERIES..... | 16 |
| 2.3. WEEKLY ALLOCATION OF HYDROLOGICAL RESOURCES | 20 |
| 2.4. ADEQUACY SIMULATIONS..... | 20 |
| 2.5. TEST CASE RESULTS | 22 |
| 3. Detection of system overloads | 24 |
| 3.1. AUTOMATIC MAPPING OF GENERATION AND CONSUMPTION ON NODES | 24 |
| 3.2. DETECTION OF OVERLOAD PROBLEMS | 24 |
| 3.3. TEST CASE RESULTS | 25 |
| 4. Reduction of the nodal initial grid according to critical branches | 26 |
| 4.1. IDENTIFICATION OF CRITICAL BRANCHES..... | 27 |
| 4.2. NETWORK PARTITION | 30 |
| 4.3. CALCULATION OF NETWORK PARAMETERS | 30 |
| 4.4. TEST CASE RESULTS | 31 |
| 5. Optimal grid expansion at the zonal level from today to 2050 | 32 |
| 5.1. SNAPSHOT SELECTION | 33 |
| 5.2. CANDIDATE SELECTION | 35 |
| 5.3. TRANSMISSION EXPANSION PLANNING OPTIMIZATION AT ZONAL LEVEL..... | 36 |
| 5.4. TEST CASE RESULTS | 38 |
| 6. Grid expansion at nodal level | 43 |
| 6.1. IDENTIFICATION OF TRANSMISSION INVESTMENT CANDIDATES | 43 |
| 6.1.1. <i>Types of transmission investments considered</i> | 44 |
| 6.2. TRANSMISSION EXPANSION AT NODAL LEVEL..... | 44 |
| 6.2.1. <i>Considering system reliability</i> | 45 |
| 6.3. TEST CASE RESULTS..... | 46 |
| 6.3.1. <i>Continuous variables</i> | 46 |
| 6.3.2. <i>Discrete variables</i> | 47 |
| 7. Robustness of the proposed architectures | 48 |
| 7.1. DC-TO-AC PROCEDURE..... | 49 |
| 7.2. VOLTAGES STABILITY ASSESSMENT..... | 50 |
| 7.3. TRANSIENT STABILITY | 50 |
| 7.4. SMALL SIGNAL STABILITY..... | 52 |
| 7.4.1. <i>Data format conversion</i> | 52 |
| 7.4.2. <i>Eigenvalue analysis</i> | 53 |
| 7.4.3. <i>SSST validation</i> | 54 |
| 7.4.4. <i>Reduced size illustrative example</i> | 55 |

- 7.5. TEST CASE RESULTS57
 - 7.5.1. Case scenario description57
 - 7.5.2. Voltages robustness.....59
- 8. Conclusions63**
- REFERENCES.....65**
- APPENDIX.....67**

List of Figures

| | |
|--|------------|
| <i>Figure 1 – Methodology proposed in e-Highway2050, WP8.....</i> | <i>iii</i> |
| <i>Figure 2 – Test case: complete initial grid (HVDC links in green, AC interconnection lines in red)</i> | <i>11</i> |
| <i>Figure 3 – Test case: initial nodal grid with 1025 nodes (HVDC links in green, AC interconnection lines in red)</i> | <i>14</i> |
| <i>Figure 4 – Yearly evolution of the capacity in maintenance for scenario 2 (on top) and scenario 3 (bottom) along with the expected net load.....</i> | <i>16</i> |
| <i>Figure 5 – Unavailable thermal capacity for any Monte-Carlo year of scenario 3.....</i> | <i>17</i> |
| <i>Figure 6 – Correlated time series of wind power generation in two zones of France (correlation of 78.7% between the de-seasonalised and de-trended series).....</i> | <i>17</i> |
| <i>Figure 7 – Correlation between the de-trended and de-seasonalised time series of wind power generation of one point in the south of Germany with the other clusters of the test case</i> | <i>18</i> |
| <i>Figure 8 – Correlation between the de-trended and de-seasonalised time series of solar generation of one point in the south of Germany with the other clusters of the test case</i> | <i>19</i> |
| <i>Figure 9 – Correlation of wind power generation between each pair of clusters in function of their distance</i> | <i>19</i> |
| <i>Figure 10 – Correlation of solar generation between each pair of clusters in function of their distance</i> | <i>20</i> |
| <i>Figure 11 – Generation schedule over one week of scenario 3 in horizon 2050</i> | <i>22</i> |
| <i>Figure 12 – Network partition according to critical branches.....</i> | <i>26</i> |
| <i>Figure 13 – Proportion of hours where a line is congested vs. average relative flow over all the simulated years</i> | <i>28</i> |
| <i>Figure 14 – Marginal severity indicator (dual value related to the line capacity constraint, relative to the maximum value) vs. average relative flow over all the simulated years</i> | <i>28</i> |
| <i>Figure 15 – Nodal price differences (relative to the maximum value) vs. average relative flow over all the simulated years</i> | <i>28</i> |
| <i>Figure 16 – Proportion of lines vs. average flow relative to maximum capacity</i> | <i>29</i> |
| <i>Figure 17 – Test case: 120 selected critical branches.....</i> | <i>29</i> |
| <i>Figure 18 – Test case: reduced zonal network (HVDC links in red).....</i> | <i>31</i> |
| <i>Figure 19 – Histograms based on the cumulative distribution of snapshots with respect to the average price differences over the system for scenario 1 (left) and scenario 2 (right) and horizon 2050.....</i> | <i>33</i> |
| <i>Figure 20 – Representation of all the snapshots from scenario 1 and horizon 2050 by plotting the scaled average price differences values against scaled standard deviation over the system</i> | <i>34</i> |
| <i>Figure 21 – Candidate selection method.....</i> | <i>36</i> |
| <i>Figure 22 – Test case: 56 selected candidates (DC candidates in red and AC candidates in green; existing PST in blue).....</i> | <i>38</i> |
| <i>Figure 23 – Test case modular development plan: each square represents a grid architecture.....</i> | <i>39</i> |

| | |
|--|-----------|
| <i>Figure 24 – Resulting zonal grid architectures after reinforcements: common development in 2030 (top-left) and all developments from 2030 to 2050 for scenario 1 (top-right), scenario 2 (bottom-left) and scenario 3 (bottom-right).....</i> | <i>40</i> |
| <i>Figure 25 – Zonal TEP results: cumulative transmission grid investments in GW for each scenario</i> | <i>41</i> |
| <i>Figure 26 – Resulting costs relative to the total cost without grid investments</i> | <i>41</i> |
| <i>Figure 27 – Zonal grid architecture in 2030 after reinforcements, with a common development for all scenarios and investment constraints</i> | <i>42</i> |
| <i>Figure 28 - Representation of the expanded network solutions</i> | <i>43</i> |
| <i>Figure 29 – Overview of the procedure of the robustness analysis.....</i> | <i>48</i> |
| <i>Figure 30 – Flowchart of the computational procedure to determine the point of voltage collapse</i> | <i>50</i> |
| <i>Figure 31 – Overview of the procedure to build the dynamic model of the system.....</i> | <i>51</i> |
| <i>Figure 32 – Overview of the critical clearing time calculation</i> | <i>51</i> |
| <i>Figure 33 – Translation from PSS/E to SSST data format</i> | <i>52</i> |
| <i>Figure 34 – HVDC link model [21].....</i> | <i>53</i> |
| <i>Figure 35 – Eigenvalue analysis.....</i> | <i>54</i> |
| <i>Figure 36 – Single line diagram of the test system to compare SSST and PowerFactory.....</i> | <i>54</i> |
| <i>Figure 37 – 24 cluster model with two VSC-HVDC links.</i> | <i>55</i> |
| <i>Figure 38 – Eigenvalues of the 24 cluster model without HVDC links</i> | <i>56</i> |
| <i>Figure 39 – Electromechanical eigenvalues of the 24 cluster model without HVDC links.....</i> | <i>56</i> |
| <i>Figure 40 – Electromechanical eigenvalues of the 24 cluster model with HVDC links.</i> | <i>57</i> |
| <i>Figure 41 – Comparison of the electromechanical eigenvalues of the 24 cluster model in terms of the difference of modal damping with and without HVDC links.</i> | <i>57</i> |
| <i>Figure 42 – Distribution of bus voltages, in pu.....</i> | <i>59</i> |
| <i>Figure 43 – Bus voltages during demand increase, without considering reactive power generation and reactive power demand variation</i> | <i>60</i> |
| <i>Figure 44 – Bus voltages during demand increase, without considering reactive power generation, and assuming constant power factor for demand</i> | <i>61</i> |
| <i>Figure 45 – Bus voltages during demand increase, considering reactive power generation and no reactive power demand variation</i> | <i>61</i> |
| <i>Figure 46 – Bus voltages during demand increase, considering reactive power generation, and assuming constant power factor for demand</i> | <i>62</i> |

List of Tables

| | |
|---|----|
| <i>Table I – Description of the system used in the test case</i> | 12 |
| <i>Table II – Description of the scenario assumptions and energy mixes for 2050</i> | 12 |
| <i>Table III – Description of the system used in the test case</i> | 14 |
| <i>Table IV – Computation times and data volumes for the generation of load/production time series for one Monte-Carlo year</i> | 23 |
| <i>Table V – Average computation times and data volumes for the simulation of one Monte-Carlo year from the generation of time series to the calculation of congestion indicators</i> | 25 |
| <i>Table VI – Description of the zonal network</i> | 31 |
| <i>Table VII – Transmission grid investments (GW) for each scenario and each time horizon</i> | 40 |
| <i>Table VIII – Computation times for the zonal transmission expansion planning</i> | 42 |
| <i>Table IX – Maximum proportion between the capacity of the reinforcements and the original one depending on the proportion of flow allowed and the number of corridors added</i> | 45 |
| <i>Table X – Zonal expansion plan requirements for the first time horizon (2030)</i> | 46 |
| <i>Table XI – Main characteristics of the nodal expansion plan obtained using continuous variables</i> | 47 |
| <i>Table XII – Main characteristics of the nodal expansion plan obtained using discrete variables</i> | 47 |
| <i>Table XIII – Comparison of eigenvalues obtained either by SSST or PowerFactory</i> | 55 |
| <i>Table XIV – Active power balance</i> | 58 |
| <i>Table XV – Reactive power balance</i> | 58 |
| <i>Table XVI – System voltages report</i> | 59 |
| <i>Table XVII – Margin to voltages collapse</i> | 60 |
| <i>Table XVIII – Computation times and output data volumes</i> | 64 |

1. Test case description

A test case of the size of the European system is used to check the feasibility of the new methodology developed in WP8, and assess the resources that would be needed to perform this kind of study. As a reminder, the purpose of this work package is not to perform a real study, such as WP2/WP4. The data used in this test case is not exact, but tries to be realistic in order to check the feasibility of the methodology on a system of the size of the European network.

1.1. *Input data: initial network and energy scenarios*

This case study is based on a 2012 HV European system. The network data was extracted from a DACF file. However, we only had geographical coordinates for some countries, including Austria, Belgium, Czech Republic, Denmark (Jutland peninsula), France, Germany, Italy, Netherlands, Portugal, Poland, Slovenia, Spain and Switzerland. The South-East of the England, including Greater London, is also represented in our test system. Thus, the initial grid, illustrated in Figure 2 and described in Table I, comprises 5155 substations and 10209 branches, among which 3 are HVDC links: two for France-UK and one for Netherlands-UK.

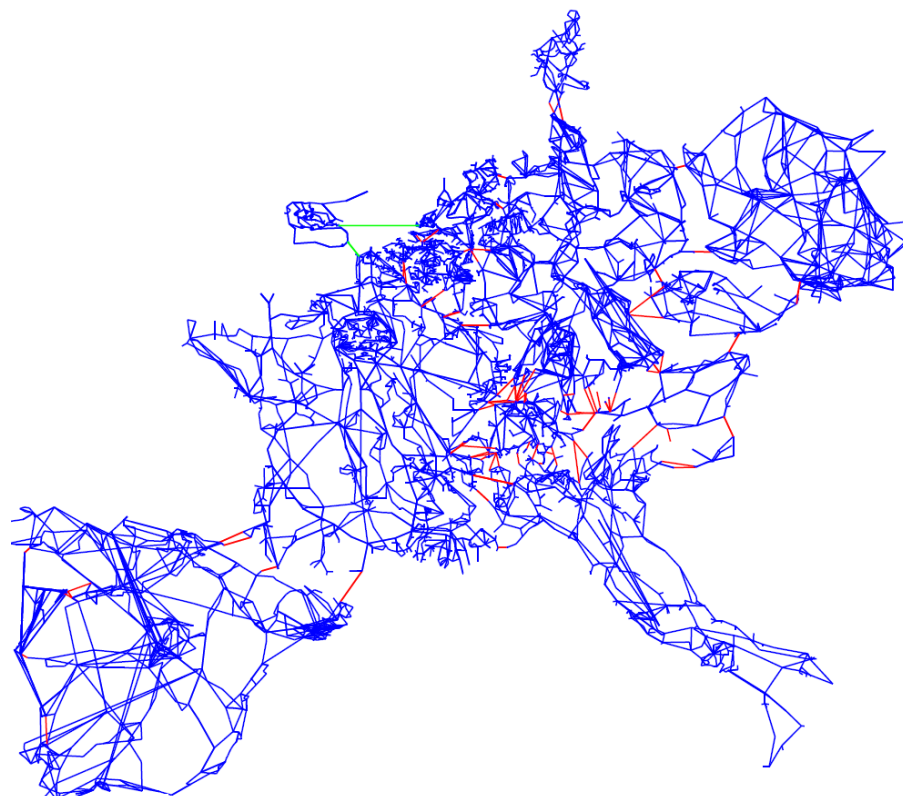


Figure 2 – Test case: complete initial grid (HVDC links in green, AC interconnection lines in red)

We consider that one substation in the input files corresponds to one node in our model. However, PST end nodes were most of the time defined by two different buses located in the same substation in the input files. Thus, by considering one substation as one node, most PSTs had identical end nodes, which is problematic in the following steps of the methodology (see PST modelling in DCOPF or TEP optimization problem). In order to solve this issue, we have split substations where PSTs were located in several nodes.

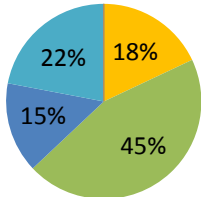
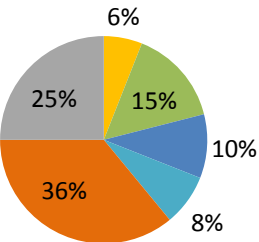
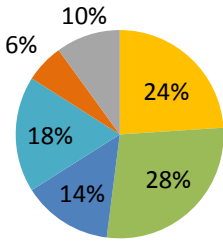
This initial system includes around 1400 generating units among which, 418 generating have their $P_{\min} > 0$. As the generating types were not indicated in the DACF files, they were attributed to fit at best the real system. Thus, the initial park is a bit different than the real one, but tries to be realistic.

Table I – Description of the system used in the test case

| | |
|---|--------------|
| Number of nodes | 5155 |
| Number of 400kV nodes | 1385 |
| Number of lines | 10209 |
| Number of 400kV PST | 17 |
| Number of 400kV interconnection lines | 69 |
| Number of HVDC links | 3 |
| Number of generating units with $P_{min} > 0$ | 418 |
| Number of hydro units with reservoir | 348 |

Then, starting from the 2012 installed capacities [11] and energy mix in the different countries, three contrasted scenarios for 2050 were built according to the following assumptions shown in Table II:

Table II – Description of the scenario assumptions and energy mixes for 2050

| | | |
|-------------------|--|--|
| Scenario 1 | 100% renewable energy: large increase in wind, solar, hydro and biomass generation Shutting down of all thermal and nuclear units |  <ul style="list-style-type: none"> ■ Solar ■ Wind ■ Hydro ■ Biomass |
| | Increase of the total annual demand by 20% Demand side management | |
| Scenario 2 | Medium (energy mix close to today with development of renewable energy sources) |  <ul style="list-style-type: none"> ■ Solar ■ Wind ■ Hydro ■ Biomass ■ Thermal ■ Nuclear |
| | Increase of the total annual demand by 30% | |
| Scenario 3 | Development of local generation (especially solar panels) Annual imports in each country should be <20% than its annual consumption |  <ul style="list-style-type: none"> ■ Solar ■ Wind ■ Hydro ■ Biomass ■ Thermal ■ Nuclear |
| | No increase of demand (same volume as 2012) | |

These scenarios are very similar to three of the scenarios studied in WP2. However, the energy mixes are slightly different than the ones from WP2 as the set of considered countries is not the same. Assumptions on

the total volume of demand and the integration of demand response are also described by these macro scenarios.

Distribution keys were calculated for each technology using the method developed in WP2 (see [4]), leading to installed capacities and annual demand by country and by scenario. Once the installed capacities of each technology and yearly consumptions have been calculated for the three scenarios in 2050, values are interpolated for 2030 and 2040.

1.2. Initial network reduction: nodal network

Detecting overload problems on a large grid is challenging since time complexity is added to spatial complexity. Using the whole existing European network (resp. the full test case system), which includes approximately 8000 nodes (resp. 5000 nodes), is unrealistic. Moreover, considering the time horizon, it would not be relevant to use the full network. The European grid must be simplified.

A network reduction method based on electrical distance was developed and presented in D8.3a [7]. It is a simple clustering algorithm which reduces the complete existing European grid to around 1000 nodes. Only 400kV nodes are kept in the simplified network and a few nodes which are electrically close are merged together. Indeed, for a long-term and large scale planning problem, we do not want to look at local issues brought by lower voltage systems, but we want to consider larger phenomena reflected by the very high voltage grid. Additional rules were also introduced in order to take into account phase-shifting transformers (PST), HVDC (High-Voltage Direct Current) links embedded in AC grid and cross-border lines. This simplification is sufficient to reduce the full network to approximately 1000 nodes. Thus, there is no need for a more complex method at this stage.

Considering our test case with approximately 5000 nodes, among which around 1400 are 400kV nodes, we obtain a reduced network with around 1000 nodes by only aggregating electrical nodes¹, lines in series or in parallel, and assigning low voltage nodes to the geographically closest 400kV nodes. Thus, we used a simplified version of the code implemented in Task 8.3, without the clustering algorithm based on electrical distances. However, the full algorithm should be used to reduce the whole European network (8000 nodes) as it enables to avoid keeping short distance 400kV lines in the reduced grid.

The resulting grid, called “nodal grid”, will be the most detailed grid model used in the following steps.

The development of the reduced nodal model was performed in two steps:

- A network partition which aggregates the nodes together. First, electrical nodes are aggregated. Then, an algorithm aggregates the 400kV AC lines which are in series or in parallel. This leads to a thousand of 400kV nodes. Lower voltage nodes are finally assigned to the closest 400kV nodes regarding geographical distances.
- The calculation of the reduced network characteristics. Classical network reduction techniques calculate the network parameters of the equivalent corridors so that inter-zonal flows in the reduced network match inter-zonal flows in the nodal network. However, at this stage of the WP8 methodology, we do not have any operational data since simulations are performed on the nodal network. Thus, we compute the reduced network parameters directly by aggregating lines characteristics from the initial network. Admittances and capacities of lines with both end nodes in different clusters are summed to get the equivalent reactances and capacities of the new corridors. This simple method is acceptable as the reduction ratio is small. 400kV PST and HVDC lines are considered separately: they are kept in the reduced network.

¹ Electrical nodes are end nodes of lines with $X \approx 0$

The obtained nodal network for the test case is illustrated in Figure 3. It is composed by around 1000 nodes and 2000 lines described in *Table III*.



Figure 3 – Test case: initial nodal grid with 1025 nodes (HVDC links in green, AC interconnection lines in red)

Table III – Description of the system used in the test case

| | |
|----------------------|------|
| Number of nodes | 1025 |
| Number of lines | 2091 |
| Number of PST | 17 |
| Number of HVDC links | 3 |

Then, starting from this initial nodal grid model, the complete methodology developed in this Work Package was tested. The process and results of each module will be detailed in the following sections. As the methodology was already presented in deliverables D8.2 to D8.5, only the main ideas will be reminded in this report.

2. Generation of production and consumption scenarios

Each of the considered time horizon and scenario is described by a set of “macro-assumptions” which is used as an input of the overall methodology. These macro-assumptions are broken down by country, such as described in the previous section. They include the assumed installed capacity of different generation sources, the expected overall demand, the possible exchanges with external countries and the integration of Demand Response.

The macro-assumptions inform about the general evolutions of the energy sector, but they do not contain the detailed mapped and operational information required by network studies. In order to have an idea of the grid capacities needed to ensure adequacy between consumption and generation, data must indeed be developed:

- under operational conditions, i.e. with actual output power of the generating units and real-time consumptions (and not total yearly consumptions), and
- for different possible situations, i.e. different moments of the year and under diverse random events.

This part of the methodology is ensured by Task 8.2 which simulates the operation of the electrical system in a copperplate model² and develops the overall assumptions, i.e. installed capacity and yearly consumption, into balanced times series of consumption and generation. The same method as the one described in D8.2a [6] has been applied in the final test case presented here, thus it will not be detailed in this section and only the main ideas will be reminded.

Some inputs of the adequacy simulator are subject to a high degree of uncertainty, while they are impacting the power system operation and its balancing. This is the case of RES generation (wind and solar generation), load, hydro inflows and outages of the generating units. A system able to supply the demand under common conditions could indeed be insufficient when facing more unusual situations (drought, cold spell, loss of a thermal unit, critical combination of intermittent RES generation, etc.). A Monte-Carlo approach has been retained to take into account the stochasticity of the problem and to study the response of the power system to diverse possible events. As a consequence, a deterministic adequacy simulation is performed on each set of stochastic inputs randomly sampled, called Monte-Carlo year. Then, the results of all the simulations are aggregated and the probabilistic properties of these results are deduced.

2.1. Maintenance scheduling

Maintenance scheduling refers to the planned stops of thermal units, such as preventive maintenance operations or refuelling.

In this first step, the maintenance calendar is planned in adequacy with the needs of the power system. The method used to generate the maintenance schedule is a simple heuristic algorithm whose goal is to plan the stops of the units so as to affect security of supply as little as possible.

The maintenance program is designed in advance and is therefore based on the expected seasonality of the stochastic inputs, on an inaccurate forecast, and not on the final exact realization of those inputs. The maintenance schedule is therefore the same for all the Monte-Carlo years and can be computed just once in the Monte-Carlo procedure.

This step is performed in parallel for each scenario and each time horizon. First, the expected seasonality of the stochastic phenomena, such as demand, wind and solar generation, and hydro inflows, is computed. This

² Without grid constraints

is based on the time series models previously built and on the inputs of the scenario: yearly demand, installed RES capacities, yearly hydro resources. Then, the maintenance schedule plans the stops of the units when the expectation of the residual load is low.

Maintenance schedules have been computed in the final test case. The total capacity in maintenance of the test case perimeter has been plotted in green, day by day, for the scenarios 2 and 3 (with different shares of RES generation) on the graphs of *Figure 4* (the considered time horizon is 2050). Residual load (blue) and capacity in maintenance (green) have opposite variations: the capacity in maintenance is logically higher when the residual load is low. On the contrary, less maintenance operations are planned when the residual load is high, as the needs for available generation capacity are more important. The comparison of the maintenance schedules for two different scenarios with more or less RES generation confirms the ability of the routine to adapt the maintenance to the specificities of each scenario and time horizon.

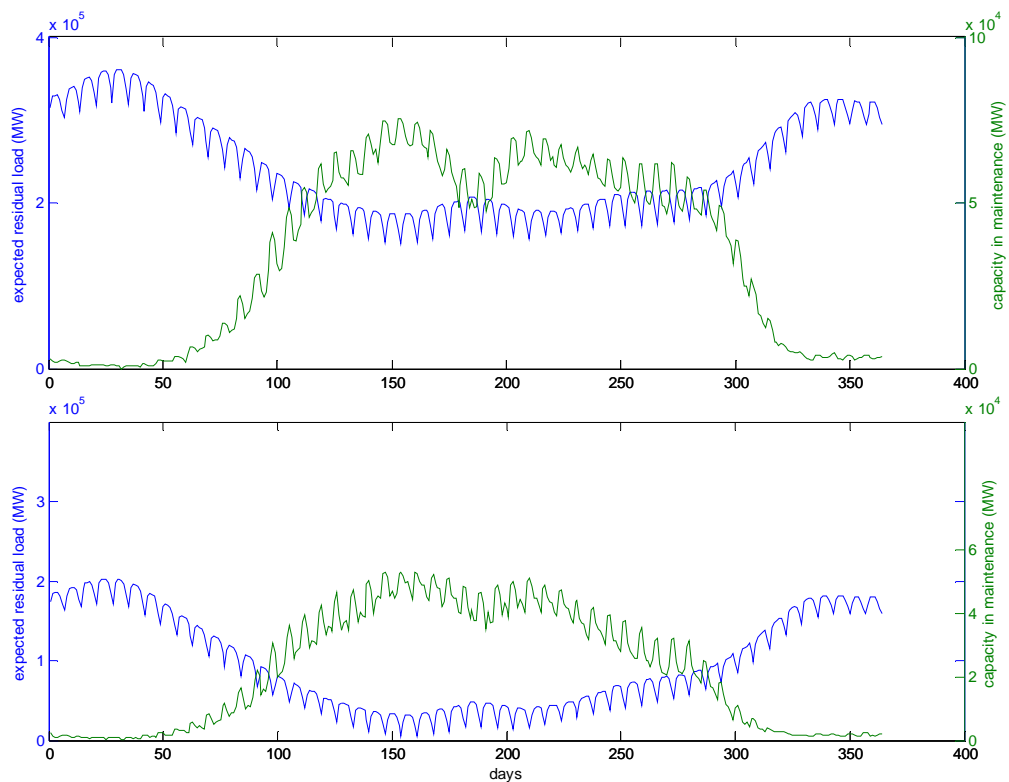


Figure 4 – Yearly evolution of the capacity in maintenance for scenario 2 (on top) and scenario 3 (bottom) along with the expected net load

In the scenario 2, the unavailable capacity due to maintenance reaches in some days more than 75 GW, that is to say 25% of the average net load. This order of magnitude is such that neglecting the maintenance of the thermal units would lead to over-optimistic adequacy assessments. Considering the loss of generation capacity due to maintenance is therefore crucial.

See section 2 of D8.2a [6] for more details on the heuristic used for maintenance scheduling.

2.2. Generation of time series

Once the maintenance of thermal units has been scheduled, Monte-Carlo samples, i.e. sets of time series which describes the yearly evolution of the stochastic inputs affecting the power system, are generated.

The outages of power plants are one of the stochastic inputs of the problem. Binary time series are generated. They describe the availability, hour per hour, of each thermal unit of the system. These time series are sampled in accordance with the outage rate and duration of the different thermal generation types.

For example, Figure 5 displays the unavailable thermal capacity for a random Monte-Carlo year, divided into the thermal units in maintenance and the thermal units under unforeseen outages.

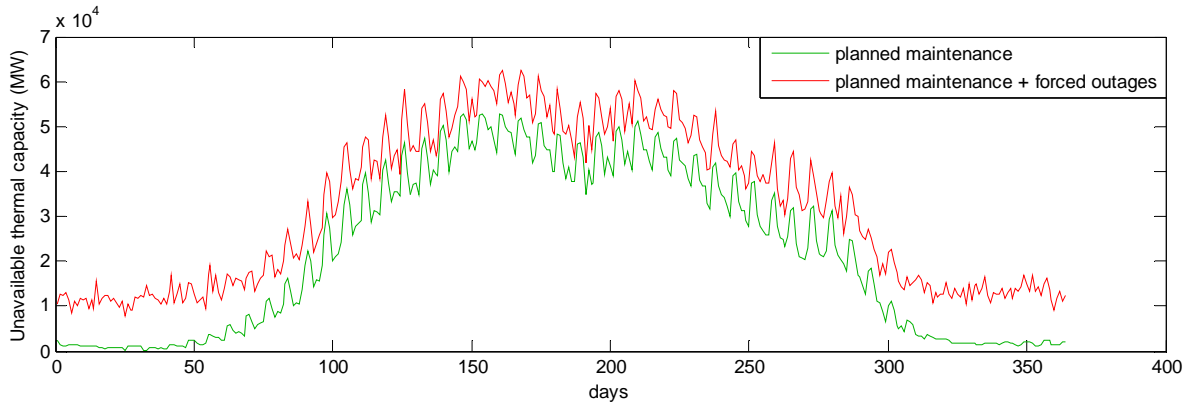


Figure 5 – Unavailable thermal capacity for any Monte-Carlo year of scenario 3

The other stochastic inputs are: the load, the onshore and offshore wind power generation, the photovoltaic (PV) generation and the hydro inflows. They are generated by a module called Time Series (TS) generator which aims at replicating the intrinsic characteristics of the considered phenomena, notably their seasonality, autocorrelation and probability density function. The newly generated time series are moreover calibrated on a new trend, which represents the assumption of the considered long-term scenario (e.g. the installed capacity of PV in 2050).

The inter-dependencies between time series are also handled by the TS generator. Indeed, spatial correlations, which are the correlations between two time series of a same phenomenon taken in two different places (e.g. wind power generation in Belgium and Denmark), were computed and considered in the final test case. As an example, Figure 6 depicts two correlated time series of wind power obtained with the TS generator.

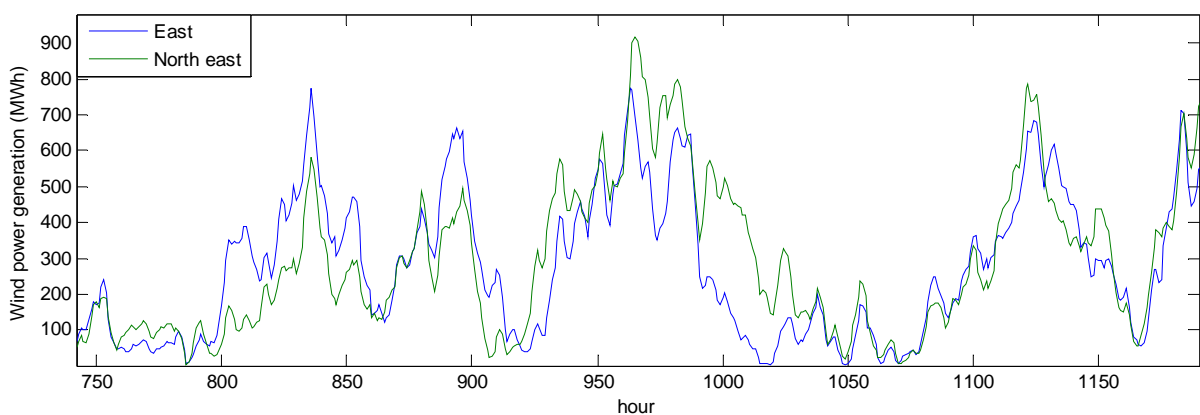


Figure 6 – Correlated time series of wind power generation in two zones of France (correlation of 78.7% between the de-seasonalised and de-trended series)

Time series of stochastic phenomena can be generated at the country level. However, to take into account the diversity of weather conditions in large countries, a smaller scale should be considered. Indeed, the wind

does not blow at the same time or with the same speed over a large territory. The same considerations can be made for the nebulosity or the temperature.

In the test case, we used the historical time series of load, solar and wind generation provided by WP2. These time series are defined at a smaller scale than the country level, i.e. for each cluster described in WP2 (see [4]). Using this data, we were able to measure spatial correlations between clusters and have a better estimation of the parameters. As presented in Figures Figure 7 to Figure 10, the spatial correlations between the time series can be significant, also on long distances across Europe. Figure 7 (resp. Figure 8) represents the spatial correlation between the de-trended and de-seasonalised time series of wind power generation (resp. solar generation) of one cluster in the South of Germany to the rest of the considered clusters. We can see that wind generation time series can be strongly correlated over a large area. Each point corresponds to the centre of a cluster of the considered study zone, and the colour of the points represents the spatial correlation between the time series (wind or solar generation) of the corresponding cluster and the reference cluster (South of Germany). The redder the point is, the higher is the spatial correlation.

Time series were then generated for load, solar, wind generation, and hydro inflows at the cluster level using the observed correlations.

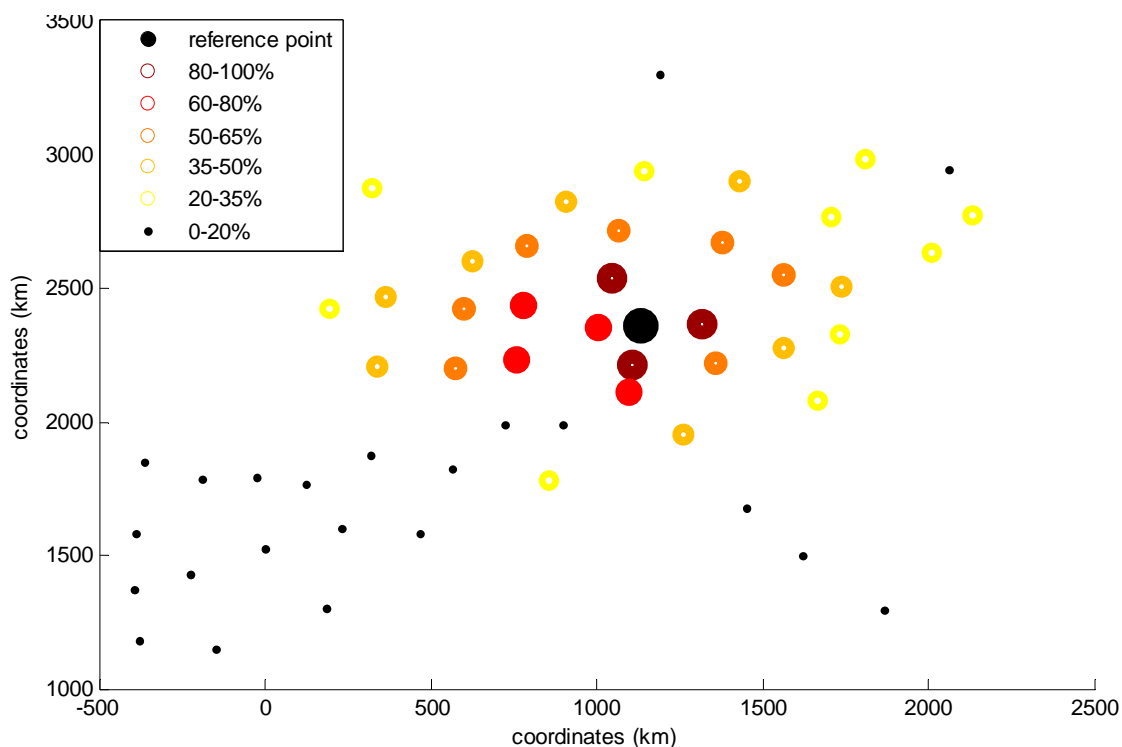


Figure 7 – Correlation between the de-trended and de-seasonalised time series of wind power generation of one point in the south of Germany with the other clusters of the test case

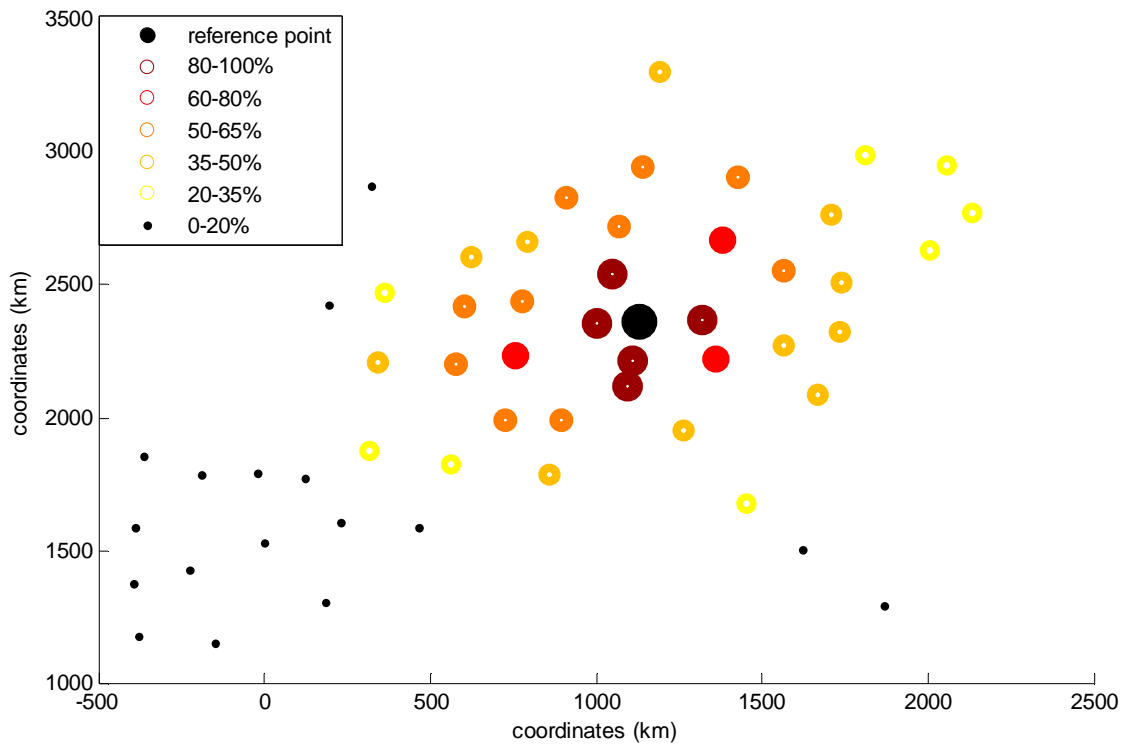


Figure 8 – Correlation between the de-trended and de-seasonalised time series of solar generation of one point in the south of Germany with the other clusters of the test case

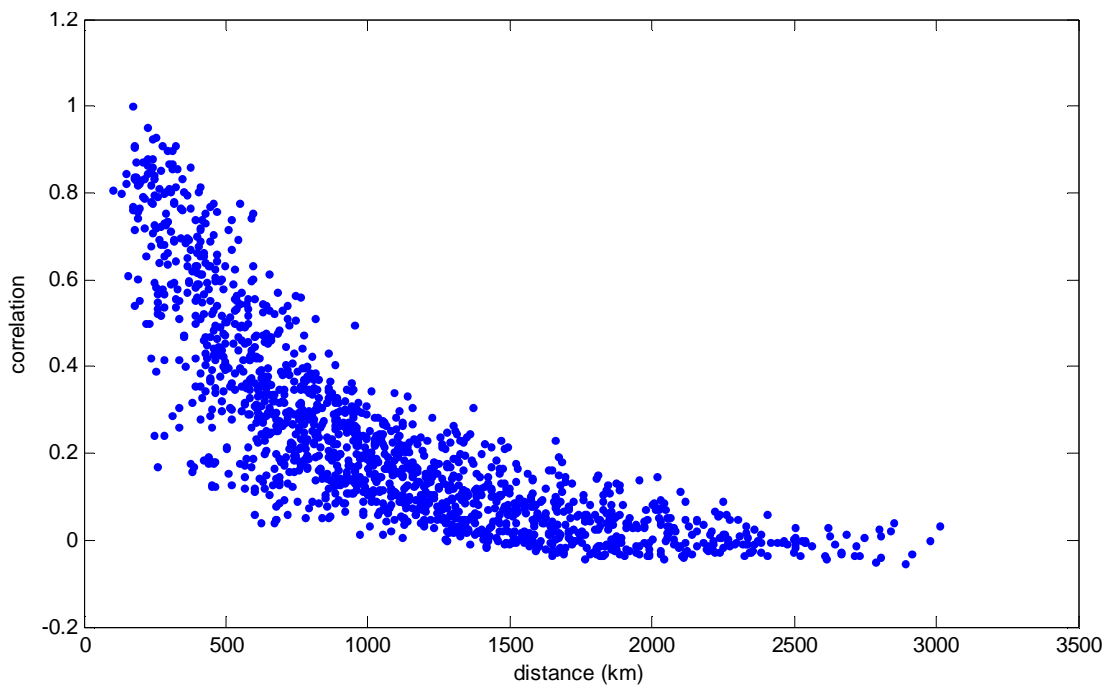


Figure 9 – Correlation of wind power generation between each pair of clusters in function of their distance

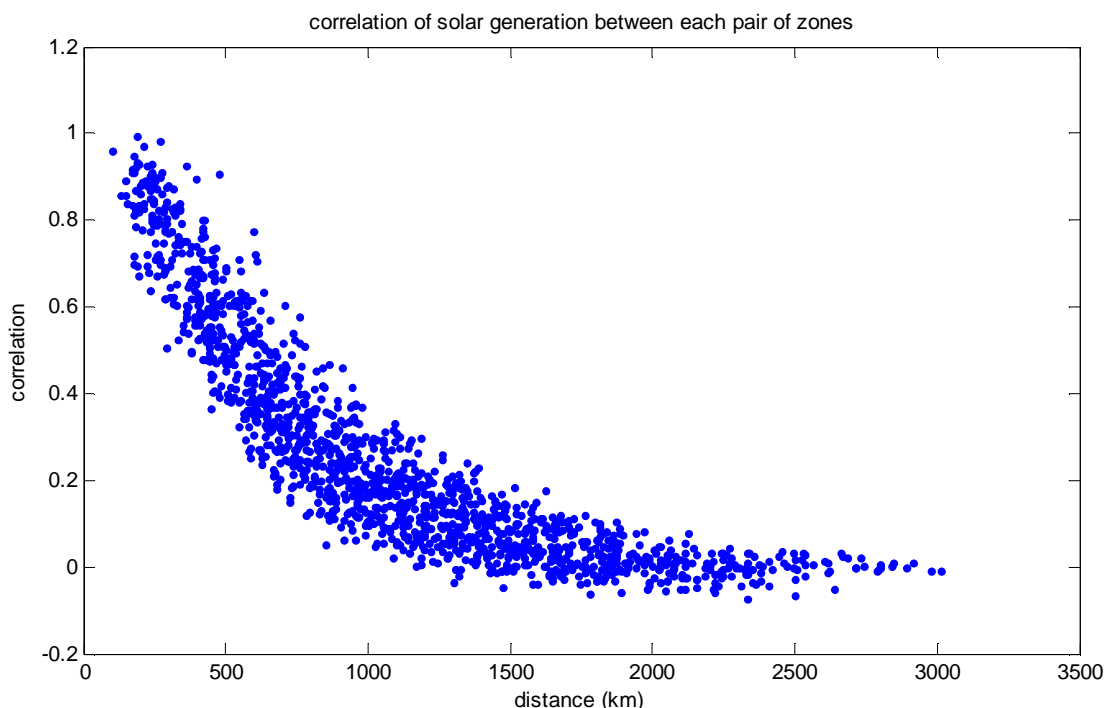


Figure 10 – Correlation of solar generation between each pair of clusters in function of their distance

See section 3 and 6 of D8.2a [6] for more details on the time series generator and the significance of spatial correlations.

2.3. Weekly allocation of hydrological resources

The goal of this next step is to allocate the yearly hydro resources among the 52 weeks of the year. It determines volume targets to be reached at the end of each week, for all the reservoirs of the system. These volume targets are the boundary conditions which will allow us to decompose the yearly adequacy problem into 52 weekly sub-problems.

This step consists in a rough adequacy problem with a weekly time step. One representative hour, with average values of generation and consumption, is used to represent each week. Hydro and thermal resources are scheduled so as to minimize the expected generation costs. The hydro resources are dispatched according to the available inflows and the capacity of the reservoirs. A simplified model is used to describe the behaviour of the thermal units and extra-European exchanges. The decrease of the thermal capacity due to the planned maintenance is taken into account.

As it is unrealistic to consider a full knowledge of the stochastic inputs on a 1-year timeframe, the allocation of the hydro energy is made through an iterative method with a 1-week foresight rolling planning. The hydro schedule is recomputed each week with the real value of the stochastic inputs of the week to come and by assuming an imperfect forecast of the stochastic inputs of the following weeks.

See section 4 of D8.2a [6] for more details on the hydro allocation method.

2.4. Adequacy simulations

Finally, detailed adequacy simulations, with an hourly time step and a finer modelling of the elements of the system are performed.

For each Monte-Carlo year, 52 simulations of 168 time steps are run iteratively. The commitment of the thermal units which are out-of-order or in maintenance is forced to zero. The volume targets obtained in the previous step are used as boundary conditions of the hydro reservoirs at the beginning and end of each week.

Simulations are run with a perfect weekly foresight: the expected seasonality of the stochastic inputs is put aside and only the real values are considered. It seems indeed reasonable to assume an accurate forecast of the load and the RES generation on such a short time horizon. In practice, the deviations from the forecast are corrected by the intra-day market, the sub-optimality due to this adjustment process will be considered insignificant in our context. This perfect foresight allows us to focus only on the technical modelling of the system and to forget the probabilistic behaviour of its operations.

Different models of thermal generating units, with varying degrees of details, have been investigated in this project in the view of selecting a homogeneous final model with a good trade-off between accuracy and complexity.

The adequacy model includes a detailed representation of the thermal units, with unit commitment, minimum stable power and minimum on-line and off-line durations. The generation costs include three components, a linear cost proportional to the output power of the unit, a constant cost which takes effect only when the unit is online and a start-up cost. A linear model is used for hydro and storage. Hydro resources are considered free, but they are limited by the bounds on the reservoirs determined in the previous step. Load can be controlled via Demand Response (DR) programs, which allow to shift a part of the load within a given delay time. Extra-European exchanges are possible and are bounded by the transmission capacities with the neighbouring countries of Europe. Import and export costs are assumed linear. Finally, the total imports of each European country can be bounded in accordance with its energy policy: weekly constraints on the import of each country have been included in the model.

The adequacy problem is therefore a large Mixed-Integer Linear Program (MILP). The problem has been solved with FicoXpress [12] for the final test case.

The model is presented in more details in section 5 of D8.2a [6].

In the test case, we considered two types of Demand Response with different participation rates for each scenario and each country. Load controllability either raises from electric vehicles or heating, with different delay times. For instance, participation rates of Demand Response range from 5 to 9% of the total demand of a country in Scenario 2 which has the most conservative DR assumptions, while they can vary from 9 to 22% in Scenario 1 which relies only on renewable energy sources and thus needs more flexibility of demand.

The previously called “extra-European exchanges” actually represent exchanges with neighbouring countries which are European countries not included in the grid model, such as Hungary, Slovakia or Sweden.

Finally, we defined different constraints on exchanges between countries depending on the national policies assumed in each scenario. For instance, import volumes should be lower than 20% of the annual demand of each country in scenario 3 (de-centralised generation close to consumption), while they can reach 50% of the total load in scenario 1 with only RES generation.

Figure 11 illustrates the generation dispatch over one week after adequacy simulations on one year of scenario 3 in 2050. The initial load is represented by the black dashed line, while the impact of Demand Response on the load can be seen on the red line. In this scenario, participation rates to Demand Response vary from 5 to 11%. We can notice that load peaks are reduced and mostly shifted from the evening to midday where PV generation is at its maximum. By increasing the demand during the periods with a low load and a high RES generation, DR also allows reducing the amount of spilled energy.

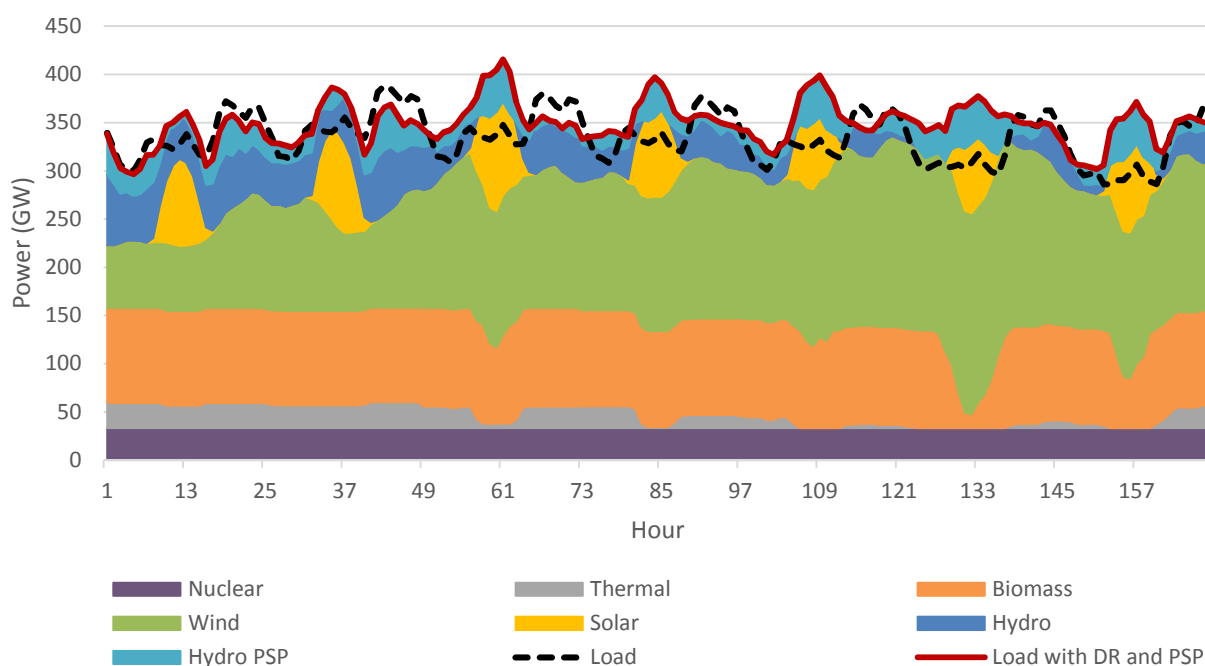


Figure 11 – Generation schedule over one week of scenario 3 in horizon 2050

The generation of uncontrollable RES, namely wind generation, solar generation and hydro Run-of-River, is the one sampled by the TS generator, which is fixed in the adequacy model. The other hydro and thermal generation sources – hydro with storage, PSP, biomass, coal and gas units – compensate the variations of the uncontrollable RES generation and consumption so as to balance the system. In the first two days, almost all the thermal units are always operated at their nominal capacity. There is a low RES generation, especially for wind. Minimum up/down times and minimum stable power constraints are rarely activated. Then, these units are shut-down when wind generation is increasing in the second part of the week.

PSP units are pumping at periods where there is excess of energy: at midday, when PV generation is at its maximum or at the end of the week when the wind generation is important and the load is low. This avoids spillage of energy. Then, PSP units redeliver this energy at load peak periods, when RES generation is low and the electricity price is higher. Thus, hydro generation brings a lot of flexibility to the system, where the share of renewable energy is high.

2.5. Test case results

We parallelized each scenario and time horizon on a different server, and the different Monte-Carlo years were run in parallel on the 16 cores of each server. The different modules described above were run successively for each Monte-Carlo year, from the generation of time series to the weekly adequacy simulations.

As a reminder, 100 Monte-Carlo years have been simulated for 3 different scenarios and 3 time horizons, resulting in 900 simulated years. Time series of load, solar, wind, hydro inflows and thermal unit outages are computed over a year, while hydro allocation and adequacy problems are run weekly. This leads to 46,800 weekly adequacy problems.

For each scenario, each time-horizon and each Monte-Carlo year, the tool returns:

- Hourly time series of uncontrollable RES and load for each country. Uncontrollable RES are: wind power generation (onshore and offshore), solar generation and hydro run of the river generation.

- Hourly time series of generation and availability of each thermal unit.
- Hourly time series of generation and water value for each controllable hydro unit (hydro with reservoir and PSP)
- Hourly time series of exchanges, imports and exports, with the extra-European countries.
- Hourly time series of system cost.

The obtained computation times and data volumes are presented in Table IV. They correspond to average values across all the 900 Monte-Carlo years simulated in the test case. Modules from the generation of time series to the identification of grid congestions (see next section) are run successively for one year, whereas up to 16 years are run in parallel on the same server.

Note that there are up to 673 generating units with $P_{min} > 0$ in the adequacy problem, which heavily impacts the number of integer variables, and the number of hydro units with reservoir management ranges from 348 to 786. This accounts for the complexity of the adequacy problem.

Table IV – Computation times and data volumes for the generation of load/production time series for one Monte-Carlo year

| | Computation time for 1 year (average across all 900 mc years) | Output data volumes for 1 year |
|--|--|---|
| Time series generator | 6min | 2.4 GB |
| Hydro scheduling | 2min | |
| Adequacy (total time for the 52 weekly MILP problems) | 2h 37min | |

3. Detection of system overloads

Once the optimal dispatch of generation has been obtained with infinite grid capacities for the different sets of stochastic inputs (wind and solar generation, load, hydro inflows, outages of thermal units) and for each scenario and time horizon, we want to quantify the congestion of transmission lines in the initial grid that would be induced by these injections. This will enable us to detect which lines are the most critical for the system across all Monte-Carlo years, scenarios and time horizons.

3.1. Automatic mapping of generation and consumption on nodes

Time series of load and non dispatchable production (solar, wind and hydro run of the river) generated for each region by the previous module described in Section 2.2 are disaggregated on each node of the simplified nodal network. This is performed regarding pre-defined distribution keys for all types of load and generation, which are an input of the methodology.

In order to compute these distribution keys, we used the method developed in WP2 (see [4]), as well as additional data on load distribution over the nodes of each country.

Thus, once adequacy simulations have been performed, this simple module disaggregates time series of load, solar, wind and hydro run of the river generation from regional level to nodal level according to the distribution keys.

We should note that dispatchable generating units are allocated on the nodal network before adequacy simulations, and considered independently in the simulations. These units are distributed in the same way than what is done in WP2 (see [4]).

3.2. Detection of overload problems

We want to quantify the congestion of transmission lines in the initial grid, while using system flexibility in the most efficient way. Flexibility can be brought by devices with no operation cost (PST or HVDC links), or associated to a cost such as re-dispatching.

Detecting overload problems on a large grid becomes challenging since time complexity is added to spatial complexity. Indeed, generation and consumption are defined with hourly time steps for a large number of Monte-Carlo years, for each scenario and time horizon, leading to thousands of injection patterns. One of the challenges is to detect which of these patterns will lead to congestions. We want to solve this problem without selecting ex-ante some representative snapshots, which does not ensure an exhaustive detection of overload problems, especially in a system with increasing uncertainties. In order to detect overload problems, the flows on the simplified nodal grid are computed for all injections using DC Optimal Power Flows (OPF) which take into account the possible network controls (HVDC, Phase Shifter Transformers (PST)). Adequacy simulations in a copperplate system (see Section 2) give the optimal dispatch of power plants which minimizes the total system cost. Each adequacy simulation is performed over one year with an hourly time step and a Monte-Carlo approach is used to take into account the stochasticity of load, intermittent renewable generation, hydro inflows and availability of thermal units. Thus, DC OPFs aim at minimizing the cost of adjusting controllable generation and load from the optimal dispatch, while complying with network constraints and using in the best way costless controls (HVDC, PST). Each DC OPF is solved independently for each time step. In the test case, 100 Monte-Carlo years are simulated per time horizon and per scenario, leading to 3,384,000 DC OPFs. Consequently, the DC OPF model should be simple and solved in a very short time.

Each DCOPF is modelled as a linear optimization problem in which controllable injections, voltage angles, PST phase angles and controllable flows over HVDC links are variables. The objective function is the minimization of the cost arising from the difference between the adjusted and the reference optimal injections. Adjustment costs of controllable generation and consumption have been defined based on priority orders. Generating units are modelled such as shut-down units can be started with an additional cost and hydro power generation stays as close as possible to the reference optimal dispatch. Indeed time dependencies are not taken into account in the DC OPF, so that adjustments of injections implying storage (e.g. hydro power plants with reservoir) should be the smallest.

Finally, each DC OPF returns indicators associated to each transmission line (e.g. flow, congestion duration or marginal cost associated to the maximum flow constraint) and nodes (e.g. marginal price). Then, deciles and average values of these indicators are calculated for each line and each node, and analysed in order to define critical branches and the zonal decomposition (see Section 4). The calculation of indicators is performed in two steps. First, average and percentiles are computed for each Monte-Carlo year, then average and deciles are deduced over all the years, scenarios and horizons.

This DC OPF model has been written in AMPL and is solved using FicoXpress solver (mixed integer solver [12]). The model is presented in more details in section 4 of D8.3a [7].

3.3. Test case results

In the considered case study, 900 Monte-Carlo years are simulated in total: 3 time horizons and 3 scenarios, with 100 Monte-Carlo years per horizon and scenario. The automatic mapping and hourly DCOPFs are run successively for each week of a Monte-Carlo year, following the generation of time series, hydro allocation and adequacy simulations. This allows us to run the years in parallel. The 9 servers we used for the simulations were composed of 16 cores each. Thus, we could run up to 16 years in parallel on the same server.

The average computation times and data volumes over the 900 simulated years, obtained using FicoXpress solver [12], are presented in Table V.

Table V – Average computation times and data volumes for the simulation of one Monte-Carlo year from the generation of time series to the calculation of congestion indicators

| | Average computation time for 1 year | Average output data volumes for 1 year |
|--|-------------------------------------|--|
| Time series generator ³ | 6min | |
| Hydro scheduling ³ | 2min | 2.4 GB |
| Adequacy (total time for the 52 weekly MILP problems) ³ | 2h 37min | |
| Disaggregation | 13min | |
| DCOPFs (total time for the 8760 hourly linear problems) | 1h 53min | 2.8 GB |
| Calculation of indicators | 5min | |
| TOTAL (1 YEAR) | ≈ 5h | 5.2 GB |

³ Modules presented in the previous section on the generation of demand/production scenarios

4. Reduction of the nodal initial grid according to critical branches

The objective of WP8 is to create an enhanced methodology to define large-scale, long-term grid architectures. However, the optimal planning of an area as large as the European system and the uncertainties involved make it impossible to solve the whole problem directly. One aspect of the strategy developed in WP8 relies on reducing the network to a simpler, equivalent model that is amenable to optimization. This is illustrated in *Figure 12*.

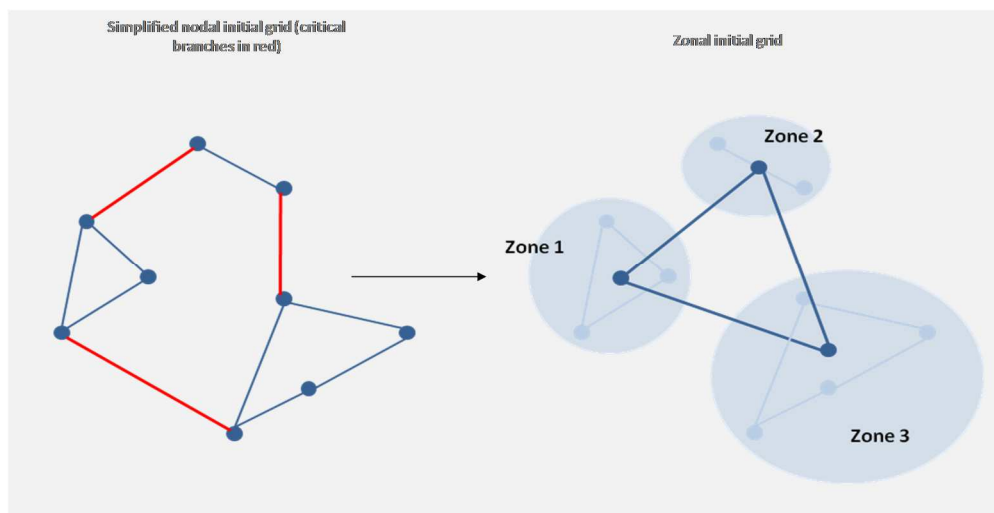


Figure 12 – Network partition according to critical branches

This section presents the method proposed to calculate an equivalent simplified zonal network from the nodal system calculated in Section 1.2. The first step in this approach is the calculation of a reduced grid where the main features of the grid are represented in the zonal model to minimize the need for internal reinforcements, and the equivalent network parameters are calculated. This zonal model will constitute the starting point for a modular network development plan.

The size of the resulting reduced zonal network (the definition of zones and corridors linking them) must be small enough to be manageable. Otherwise, optimizing the grid expansion over some decades, for several scenarios would not be possible. Although the developed method is flexible in terms of number of nodes, the target size for the European system is about 100 zones for the European System, which we believe to be manageable for TEP but still be able to capture adequately the most important features of the network. Therefore, the objective of this task is to define and develop a network reduction technique able to simplify the model of the European network that has been developed in the initial reduction step in the order of 1000 nodes, to about 100 zones or between 150 and 200 corridors. This reduced network should be able to reproduce the behaviour of the original detailed network with a high enough level of accuracy. This means that, to the extent possible, the inter-zonal flows of the original nodal network, including the flows on the identified critical branches, should approximate those in the equivalent zonal network for all the scenarios and time horizons considered.

The development of a reduced model comprises two subproblems:

1. First, network partition assigns nodes into zones. This partition should preserve, to the extent possible, all critical branches. That is, the end nodes of critical branches should belong to different zones. Besides, it should assign nodes that are electrically and geographically close to the same partition, in order to keep long corridors in the reduced network.

2. Then, network reduction creates a zonal network that approximates the characteristics of the original system as close as possible, including inter-zonal flows and losses.

Ideally, these two subproblems should be performed simultaneously to find the partition resulting in the best reduced system. That is, we should solve an optimization problem for network partition and reduction concurrently. However, the unmanageability of this problem leads us to approaching each phase independently.

4.1. Identification of critical branches

First, copperplate and transmission-constrained simulations of the European power system allow identifying the most important congestions in the network for a wide set of possible evolutions of the system. These congested lines, together with flow controlling devices such as HVDC lines or PSTs make up the critical branches, which are used as the key element in the reduction.

We define critical branches as the transmission lines that present a special interest for the purposes of TEP. Possible reasons for this special interest are, for instance:

- Frequent congestions. If a line is congested, it will impose operation constraints that would be ignored if the line was internal to a zone. That is particularly important given that congestion is one of the main drivers of transmission expansion decisions. It should be noted that congestions on very short lines are not considered.
- Some power flow control devices, such as HVDC lines or PSTs. These elements should be modelled individually in order to capture the flexibility they bring to the operation of the system.

We propose several criteria for the identification of these critical branches:

- The average flow relative to the maximum capacity of a line, which captures concisely the utilization of a transmission line.
- However, even if a line supports a high average flow, increasing its capacity will not generally result in operation savings unless the line is already congested. Therefore, we propose to use the proportion of operation hours where the line is congested as an indicator to complement average flow.

The economic impact of a congestion in two different lines can be very different. In order to filter the congested branches with the highest economic consequences, we propose to study the two following indicators:

- The value of the dual variable of the capacity limit constraints considered when solving the power flow, weighted across periods and scenarios.
- The difference between the nodal prices at the extremes of the line weighted with the line flow across periods and scenarios.

Once calculated in the test case over the 900 Monte-Carlo years, we found that there was a considerable overlap among indicators. The branches that have a high average relative flow tend to be congested a large proportion of hours and have high congestion severity indicators. These relationships among indicators are illustrated in *Figure 13*, *Figure 14* and *Figure 15*. There is a high correlation (around 70%) between the average relative flow and the proportion of hours where a line is congested, and we can notice that by selecting all the lines which have an average relative flow higher than 60% of their capacity, we keep the branches which are congested most of the time (more than 50% over the 3,384,000 hourly DCOPFs). The same observation can be made for the two other congestion severity indicators: the lines with the highest average relative flow correspond to the ones with the largest severity indicators. Thus, selecting critical branches based on the average relative flow seems to be relevant.

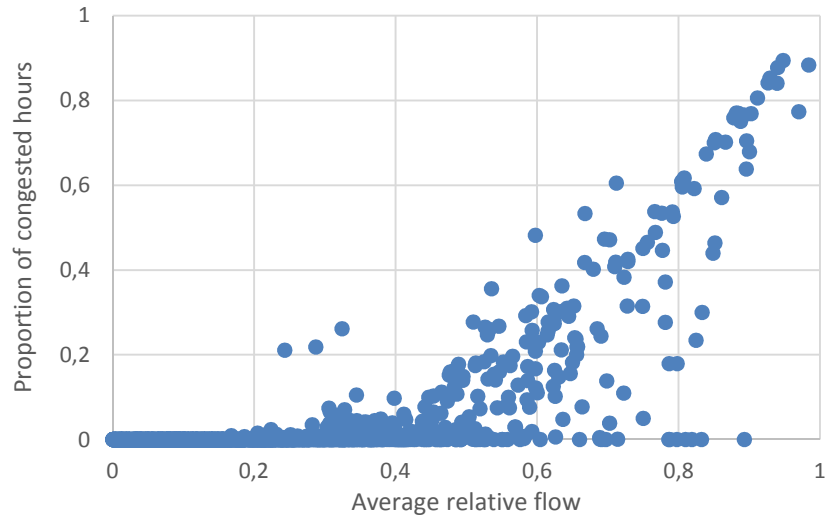


Figure 13 – Proportion of hours where a line is congested vs. average relative flow over all the simulated years

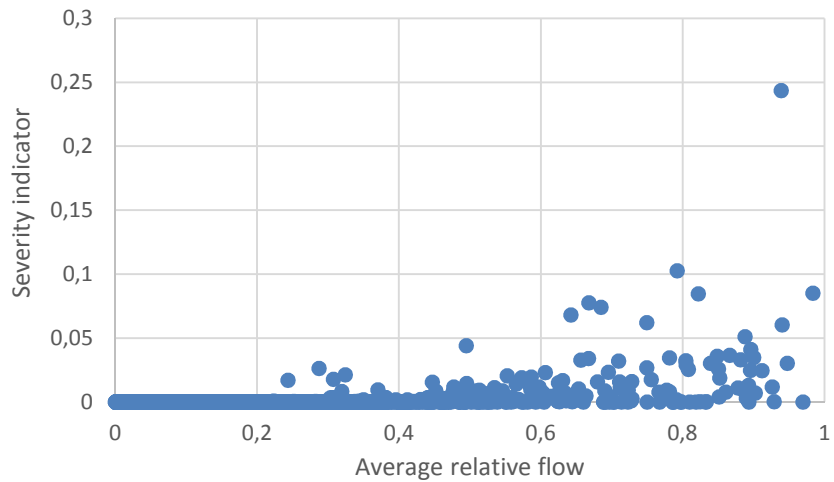


Figure 14 – Marginal severity indicator (dual value related to the line capacity constraint, relative to the maximum value) vs. average relative flow over all the simulated years

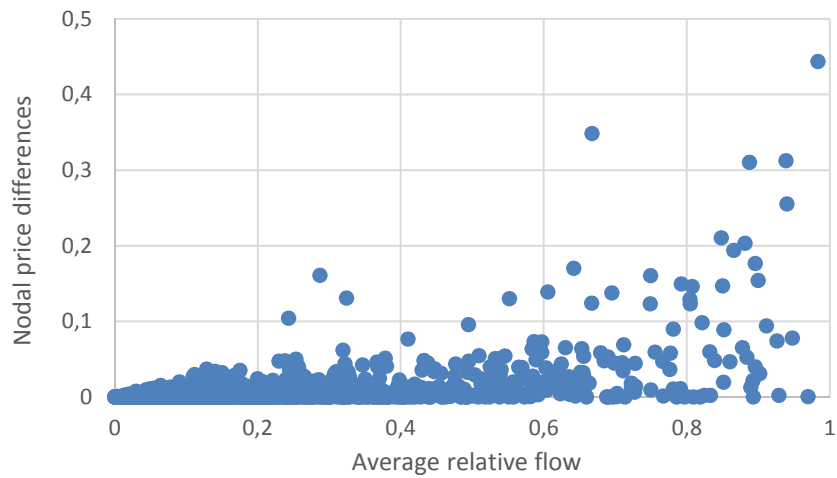


Figure 15 – Nodal price differences (relative to the maximum value) vs. average relative flow over all the simulated years

Thanks to the previous results, we decided to keep the average flow as the main indicator for critical branches selection. These indicators are calculated for each branch of the nodal network, over all the 3,384,000 hourly DCOPFs. Then, we classify the branches from the most loaded to the lowest and we keep the 100 first lines as critical branches. *Figure 16* shows the cumulative distribution of the average flow relative to line capacities over all the calculated indicators. 5% of the transmission lines in the test case, corresponding to around 100 branches, support an average flow above 60% of their maximum capacity.

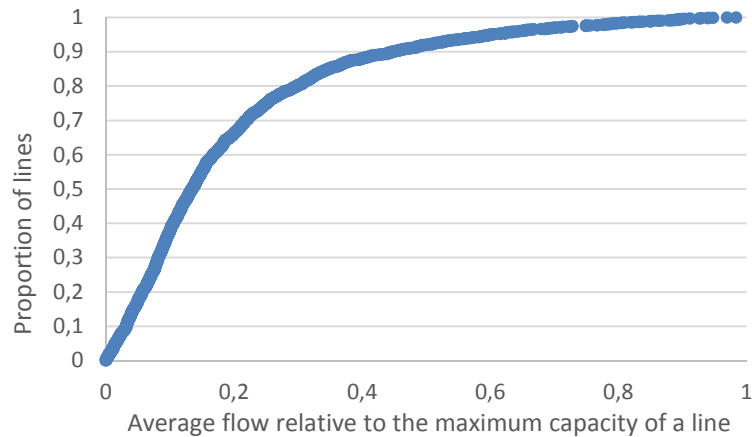


Figure 16 – Proportion of lines vs. average flow relative to maximum capacity

As this reduction is performed directly on the nodal network, which is already a reduced model of the initial European grid, there should not be very short lines. However, in the test case, most of the 400kV nodes are kept in the nodal grid to reach 1000 nodes. Thus some short lines can still persist in the nodal grid. In order to avoid short distance critical lines, a filter was first applied to remove very short lines from the critical branches selection. The 120 critical branches selected in the test case are illustrated in *Figure 17*: 100 of them correspond to the most loaded lines over all the simulated years, while the 20 others correspond to the PSTs and HVDC lines. We can notice that those critical branches are located all over the network, and are not only cross-border lines.

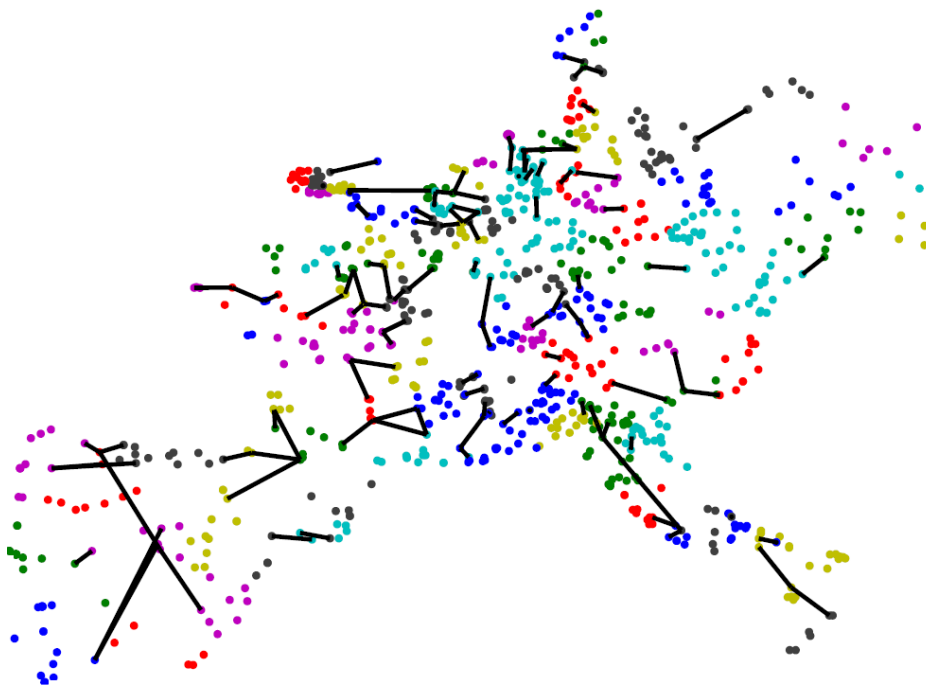


Figure 17 – Test case: 120 selected critical branches

4.2. Network partition

A heuristic algorithm builds an initial partition by starting with a single zone that is potentially split as many times as critical branches have been identified:

- If both extremes of a critical branch belong to the same zone, this zone is split in two new zones.
- The nodes that belong to the split zone are reassigned to the subzone, between the two created, that is closest to these nodes in terms of composite distance.

This simple algorithm ensures that critical branches are represented explicitly in the partition and incorporates all the information that has been considered relevant for the composite distance calculation.

This initial partition is subsequently refined by a clustering algorithm (*k*-medoids), based on a composite distance which is 50% electrical distance and 50% geographical distance. The reasons why a composite distance is used are detailed in Section 5 of D8.3.a [7].

Finally, we define the final representative node of each zone as the most connected node, which is the node that has the highest connection capacity to the rest of the network. This guarantees that the representatives will be relatively important nodes in the network, such as large power plants or highly connected substations. The representative nodes are the ones kept in the reduced network to represent their related zone.

4.3. Calculation of network parameters

Once the zones in the reduced network have been computed, we need to calculate the parameters that describe the corridors among them. These parameters are the equivalent reactances and physical capacities of the corridors of the reduced network. The objective is to compute a unique reduced equivalent network. Therefore, the parameters computed must be unique, that is, they must be independent of the operation situations.

For this task, we follow an approach based on reference [22], where the authors define inter-zonal corridors as the equivalents of the sets of lines connecting pairs of zones in the nodal network model. These inter-zonal corridors are both the critical and not critical branches previously used for the network reduction.

The main idea followed to calculate the network parameters of the corridors is that inter-zonal flows in the reduced network must match the inter-zonal flows in the nodal network. Due to the different characteristics of the equivalent reactances and physical capacities of the corridors, we have employed two different methodologies to compute them. These methodologies are detailed in Section 5 of D8.3.a [7].

The methods used in the test case for equivalent network parameters calculation are unfortunately not the ones presented in D8.3.a, but consist of a simpler method which was easier and faster to implement. Indeed, at the time of simulations, the equivalent capacity module was not totally ready to be integrated to the other modules, and due to the lack of time we used a more naïve method. This alternative sums the capacities and reactances of the inter-zonal lines to compute the corridors characteristics. Thus, equivalent capacities are a bit over estimated: the sum of inter-zonal capacities is an upper bound to the equivalent physical capacity. This will lead to less investments in the TEP, but this allowed us to continue running the methodology.

4.4. Test case results

The obtained reduced 100-zone network from the test case is illustrated in *Figure 18*. This network reduction was based on 100 critical branches selected following 3,384,000 hourly DCOPFs. It is composed of 100 zones, 243 corridors among which 3 HVDC lines and 17 PSTs (Table VI).



Figure 18 – Test case: reduced zonal network (HVDC links in red)

Table VI – Description of the zonal network

| | |
|----------------------|-----|
| Number of zones | 100 |
| Number of corridors | 243 |
| Number of PST | 17 |
| Number of HVDC links | 3 |

In contrary to the previous modules which were run in parallel for each Monte-Carlo year, this step is run once for all scenarios and time horizons considering all the indicators. It took one minute to compute the reduced network, and 13 minutes to calculate the indicators over all the simulated years.

5. Optimal grid expansion at the zonal level from today to 2050

The purpose of Transmission Expansion Planning (TEP) is to provide grid expansion candidates that will allow the grid to take advantage of most of the generating units while reducing the load curtailments at a minimal investment cost. It is a trade-off between minimizing the investment costs and minimizing the generation and load curtailment costs.

Before optimizing the TEP, two components must be defined: the candidates in which the model is allowed to invest and the snapshots on which the impacts on system operation are assessed. Nowadays most of the TEP methods consider that candidates are provided by experts based on which corridors need reinforcements and where should the most profitable candidates be built. The snapshots are also defined manually and usually reflect the system critical states based on the variations of load and intermittent generation like wind or solar on a few situations: those states usually only describe worst case scenarios or high and low load situations. Both processes can introduce flaws in the problem's definition and then result in suboptimal solutions:

- Hand-picking the candidates prevents us from testing candidates that would become profitable once others have already been implemented. This is even more important when the TEP problem is solved over a long period with several time-horizons: it becomes difficult to estimate the profitability of a candidate without a proper methodology.
- If the chosen snapshots are only based on critical situations, they can lead to pessimistic estimations of operations and over-investment.

For both components we believe that a rigorous methodology should be followed: potential candidates should be chosen for their feasibility and profitability while representative snapshots should be chosen to reflect as much as possible the actual operations of the grid.

The TEP optimization in itself is often considered as a two stages problem where the investments are first optimized and then the operations are calculated through an Optimal Power Flow constrained by the previously optimized transfer capacities. This decomposition can be suited when the goal is to plan a "one-step" development of the grid, where the decision variables are optimized only for the target year and the following years are not considered. However when several time-horizons are considered within the span of the study period, it cannot be solved one horizon at a time: all horizons must be taken into account to dynamically optimize the development of the grid.

Because grid evolution is a long administrative and technical process, Transmission System Operators usually plan their future expansions 10 years ahead: the grid development cannot be optimized independently for each scenario and we consider that TEP in the first time horizons (up to 2030) should be common to all scenarios. For that purpose we present a formulation of the TEP problem as a single optimization over all the scenarios and all the time-horizons.

We propose to perform the different processes in the following order:

- Snapshot selection: find representative snapshots among hourly simulations of the grid
- Candidate selection: choose profitable candidates based on the operational savings they could bring (calculated on the selected snapshots)
- TEP optimization: optimize when and how much the candidates should be invested in (operational consequences of investments are calculated on the selected snapshots)

The whole TEP process is described in deliverable D8.4a [8].

5.1. Snapshot selection

The aim of the snapshot selection is to find a relatively small number of snapshots to represent the whole pool of grid simulations (not only critical situations) so that operational expenses can be estimated. To be consistent, the selected snapshots should lead to similar grid investments as when the TEP is run with the whole pool of snapshots. We defined a selection method based on a k -medoids clustering algorithm. In contrast to the k -means algorithm, k -medoids chooses data points as representatives of the clusters. The reasons of our choice are detailed in Section 2 of D8.4a [8].

In a power system, the features can be of various natures: balance-related (load, wind or solar generation), congestion-related (congestion duration, load shedding) etc. We decided to use price differences between zones to assess the similarity between the snapshots in the test case, although more features can be studied (see D8.4a [8]). Zonal price differences can give a feeling of the congestion on the corresponding line and are triggers for investment in new lines.

Price-differences are local values: each clustering feature is associated to a pair of zones. Thus, the number of features is exponential when the size of the system grows: we propose to replace local features by geographical statistical indicators, such as the average of zonal price differences values over the system, their standard deviation, and the minimum and maximum values. These statistical features appeared to give similar expansion results to the ones obtained with local features in the results of D8.4a [8].

Figure 19 illustrates the distribution of snapshots with respect to the average zonal price differences over the system. The values have been scaled so that for each set, the mean over all the snapshots is 0 and the variance is 1. Each histogram represents all the 876,000 simulated snapshots – 8760 hours x 100 Monte-Carlo years – of scenario 1 (left) and scenario 2 (right) for horizon 2050. We can notice most snapshots have similar average price differences values in scenario 1, while they are more distributed in scenario 2.

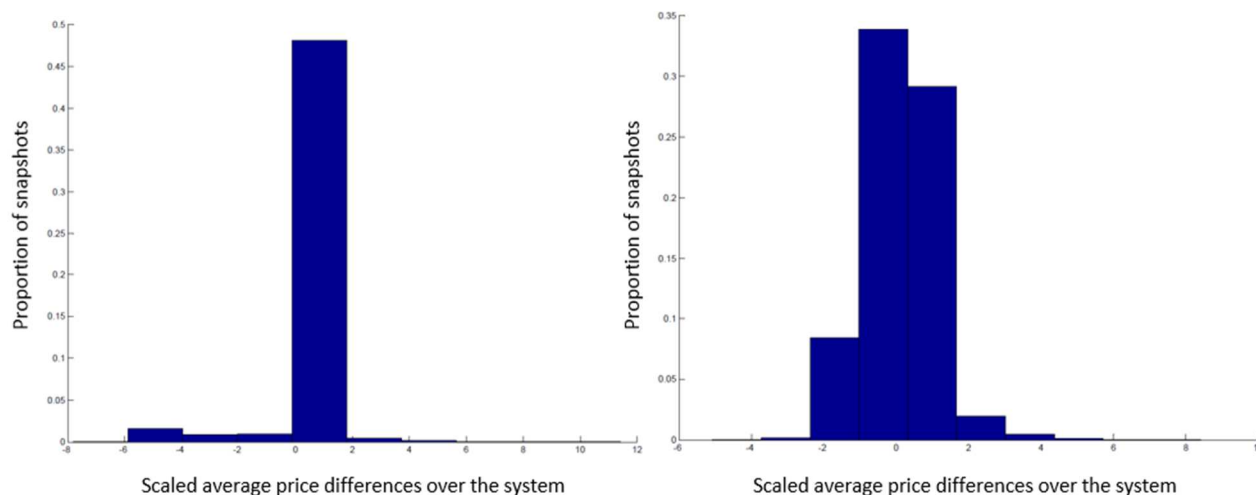


Figure 19 – Histograms based on the cumulative distribution of snapshots with respect to the average price differences over the system for scenario 1 (left) and scenario 2 (right) and horizon 2050

Although all snapshots from scenario 1 and horizon 2050 seem to present close price differences if we only consider the average values over the system, it is not the case anymore when taking into account another statistical parameter such as the standard deviation of price differences values as shown in Figure 20.

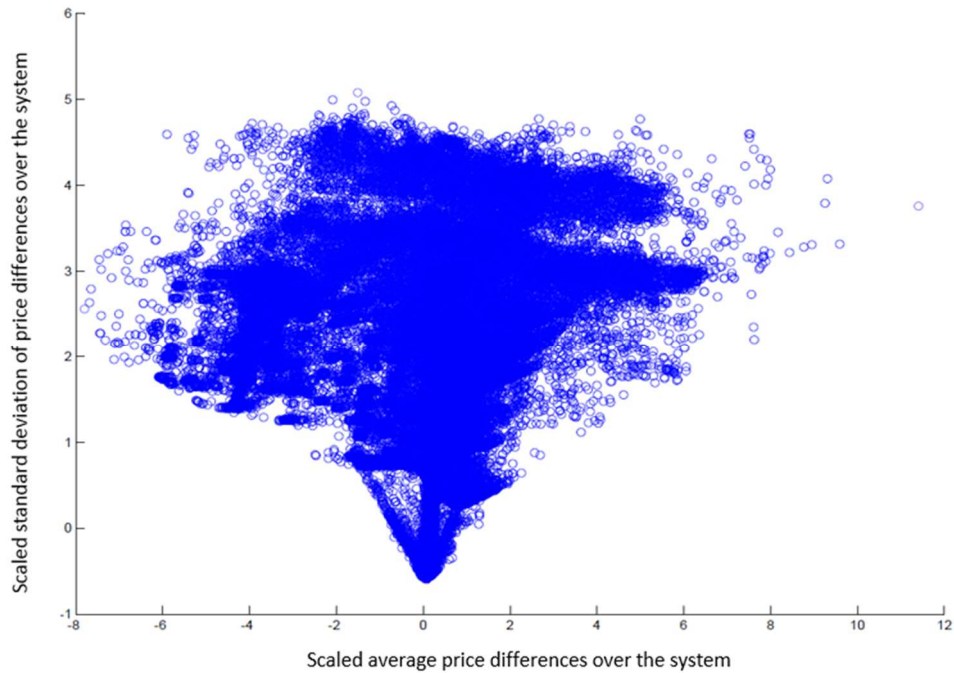


Figure 20 – Representation of all the snapshots from scenario 1 and horizon 2050 by plotting the scaled average price differences values against scaled standard deviation over the system

In our methodology, we consider that zonal price differences are provided by an external process: to obtain the zonal prices, a DC Optimal Power Flow has to be run on the zonal network. The same model as the one described in Section 3 was used. However, the grid considered in this step is the reduced zonal network and not the nodal grid model.

Several k -medoids clustering algorithms were tested in the final test case. Indeed, it was the first time we had to deal with such an amount of data to cluster (876,000 snapshots), and the implemented prototype was not designed for this complexity. The most time consuming part of the k -medoids clustering is the calculation of the distances between snapshots to find the medoids. In the Partitioning Around Medoids (*PAM*) algorithm [13], which is the most common realization of the k -medoids clustering, all pair-wise distances between snapshots are stored in the central memory, thereby consuming $O(n^2)$ memory space. Thus it is not efficient with large data sets such the ones we are dealing with. Kaufman & Rousseeuw [14] suggested the *CLARA* (Clustering for Large Applications) algorithm, which extends the k -medoids approach to larger data sets. It draws multiple samples of the data set, applies *PAM* on each sample and gives the best clustering solution. Since *CLARA* has a sampling approach, the quality of its clustering results depends on the size of the sample. Thus, we need to find a good compromise between the efficiency in clustering large data sets and the clustering quality. Finally, the *CLARANS* (Clustering Algorithm based on Randomized Search) algorithm was proposed by Ng and Han [20]: it is more efficient and scalable than both *PAM* and *CLARA*. By testing successively the different k -medoids algorithms in our test case, we were able to run the snapshot selection from several days (quadratic complexity using *PAM*) to a few minutes. This has been simulated with R and Python, however other languages should be benchmarked. Computation times are presented in Section 5.4.

We would ideally consider all the simulated snapshots in the TEP optimization. Since this would lead to an unaffordable complex TEP problem, it is necessary to find a trade-off between the representativeness of the selected snapshots, and thus have a large enough set of snapshots, and the computational complexity of the TEP problem. At the time of simulating the test case, the implemented prototype enabled us to run the zonal TEP problem with only 5 snapshots per scenario and time horizon within a reasonable time. In other words, we selected 5 snapshots to represent 100 Monte-Carlo years, i.e. 876,000 hours. This number of selected

snapshots is a bit too low, however we believe that further work on the TEP modelling taking advantage of MILP solvers improvements would enable to increase the number of selected snapshots.

5.2. Candidate selection

In order to reduce the computation time of the Transmission Expansion Planning (TEP) optimization we also want to reduce the number of candidates proposed to the optimization. Without this candidate selection, the optimization would have to deal with thousands of candidates (and all the combination possibilities) for the grid expansion.

In the test case, whose zonal network model is composed of 100 zones, there are $\frac{99 \times 100}{2}$ pairs of zones, which lead to 9900 possible candidates if only 2 corridor types are considered. Many of those initial candidates are not technically feasible (too long connections, land-use constraints...) and many of the feasible ones are not profitable because they cost more than the potential benefit they can bring. The proposed method operates as a filter by sorting the feasible and profitable candidates out of the initial pool.

Since the TEP optimization considers several scenarios and time horizons, we propose to find the final pool of candidates by merging the final pools related to each scenario and time horizon: this makes the common development in the first time horizons easier and allows the optimization to pick candidates in a broader pool and find unexpected investments.

Based on the work of Lumbreras, Ramos and Sanchez [16], this method can be divided into three main processes: identification of the feasible candidates, candidate management and candidate analysis. The first process analyses the initial pool of candidates and removes any candidate which violates a technical constraint: in the test case we only consider the length of the candidate. The second process iteratively checks the profitability of the feasible candidates, identifies the candidates to install (simplified TEP on the most profitable candidates), and installs them in the grid. When no new candidates are installed, the candidate analysis is performed to find complementary or substitute candidates among the profitable candidates which have not been invested in.

The following figure explains how the three processes are performed. The method is designed so that candidates are selected for each time horizon and each scenario and then the final candidate pool is obtained by merging the individual pools: this allows the subsequent TEP optimization to use candidates in a time horizon even though they were not specifically discovered for it and it helps the parallelization when implementing the methodology (the candidate selection is parallelized for each scenario and each time horizon). This method is detailed in Section 3 of D8.4a [8].

To speed up the relaxed TEP used in the candidate management step, we tested several options of the FicoXpress solver [12]. For instance, the automatic scaling option enabled us to divide the total computation time by 4. Indeed, the TEP problem contains numerical values with very different orders of magnitude, hence the need to rescale the matrix.

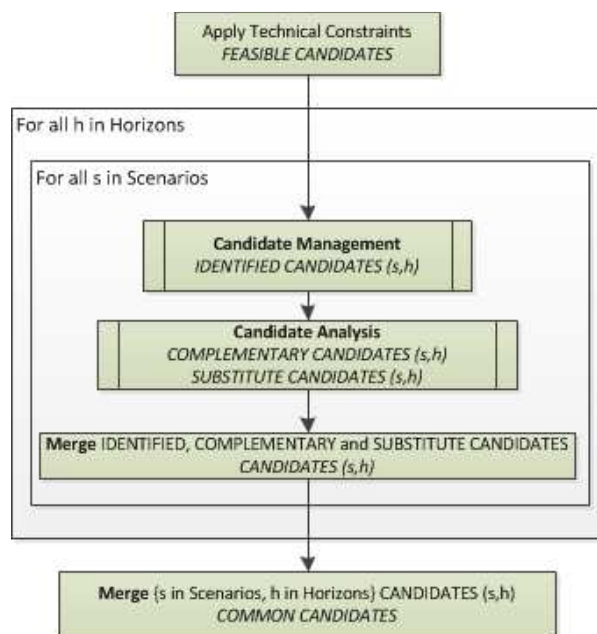


Figure 21 – Candidate selection method

With regard to the test case, technological data for AC and DC lines was collected from WP3 (see [7]), such as reactance per unit length, capacity, maximum length of the line, investment cost or operation and maintenance costs. Conversion stations were also considered in the HVDC model.

5.3. Transmission expansion planning optimization at zonal level

The purpose of our methodology is to decide in each scenario and time horizon which candidates are the most beneficial under operational constraints. We assess the cost implied by the investment in each candidate but also the impacts on system operation that we can expect. We consider that the ideal situation is when production and consumption in each zone are at their "copperplate" level: the operational consequences of reinforcements are the cost of deviation from these ideal injections. Once an investment has been decided, we model the impacts on system operation as the difference between the costs of operating with and without the grid (obtained from the adequacy module described in Section 2). Therefore, an investment is profitable if its cost and its operational consequences are lower than the operational consequences of not investing. The expansion stops when there is not more profitable solutions or when the operational cost has reached the copperplate solution. However we can also consider that for each time horizon and each scenario, investments cannot be higher than a fixed limit: this maximum investment could be arbitrarily defined or based on the difference between the expected operational cost with the initial grid and the copperplate cost for the considered time horizon and scenario.

Since the desired methodology should handle several scenarios, we formulate the problem with scenario weights so that every scenario can be considered in the same optimization. Every time horizon is also taken into account so that the developments of a given time horizon depend on the optimal development of the previous ones: this is the modular development plan.

Also, because grid evolution is a long administrative and technical process, Transmission System Operators usually plan their future expansions 10 years ahead: we consider that Transmission Expansion Planning in the first time horizons (the first 10 years of the study period) should be common to all scenarios.

We present a high-level formulation of the TEP problem as a bi-level optimization over all the scenarios and all the time-horizons in the following problem.

$$\min_{NewG} \sum_{s,h} w_s \cdot (CAPEX(NewG_{s,h}) + E_{r \in \mathcal{R}(s,h)} [OPEX_r(TotalG_{s,h})])$$

subject to:

$$CAPEX(NewG_{s,h}) \leq InvMax_{s,h}$$

$$TotalCap_{s,h} = TotalCap_{s,h-h_{step}} + NewCap_{s,h}$$

$$TotalY_{s,h} = TotalY_{s,h-h_{step}} + NewY_{s,h}$$

$$OPEX_r(TotalG_{s,h}) = \min_r VarCost(I^r, I_0^r)$$

subject to:

$$|Flows(I^r)| \leq TotalCap_{s,h}$$

$$LocalBalance(I^r) = 0$$

$$ACFlows(I^r) = Angles(I^r) \cdot TotalY_{s,h}$$

In this simple formulation, $E_{r \in \mathcal{R}(s,h)}$ is the expectation over the snapshots related to the considered scenario and time horizon. I^r is the optimal dispatch of generating units allowed by the grid in snapshot r . The objective of the second optimization is to match the optimal dispatch with the reference dispatch I_0^r ("copperplate" injection dispatch in the snapshot r) by minimizing the variation cost caused by this dispatch modification.

From this high-level description and since investments only depend on the equipment ($NewG_{s,h}$), we can split the problem into two levels:

- Investment Level (1st optimal function), where only the grid is optimized,
- Operational Level (2nd optimal function), where the injections are optimized and constrained by the grid.

When those two levels are combined, products between decision variables and angle variables appear: a basic formulation of the full optimization becomes non-linear. Since the considered products relate to integer variables on the one hand and continuous variables on the other hand, we can easily modify the formulation through a "disjunctive model" [2] so that the optimization can be written as a Mixed Integer Linear Programming problem. The mathematical formulation of the TEP problem and this modification are detailed in Section 4 of D8.4a [8].

The TEP problem has been implemented in AMPL [1], using FicoXpress solver [12]. Several options have been tested to speed up the resolution of the problem, such as the number of threads allocated to the simplex (primal, dual and barrier solves). We were finally able to run the TEP optimization within a reasonable time (between one and two hours) for 45 snapshots and 56 candidates. The resolution of the TEP problem with maximum investment constraints took more time: around 5 hours. It should be noted that with more computational power and further improvement of codes, the TEP could be run over more snapshots.

5.4. Test case results

First of all, hourly DCOPFs are run on the zonal network to compute zonal prices: they correspond to dual values associated to the balance constraint in each zone. This step is very similar to the previous DCOPFs described in Section 3, although it is faster as the considered network size is reduced by a factor 10. Then, the statistical zonal price-differences values are computed over the system for each hour. For instance, the average value of all zonal price-differences is calculated for each hourly step. The same is done for minimum, maximum and standard deviation values. This step is performed in parallel for each year.

Then, we launched the selection of snapshots: 5 snapshots are kept by scenario and horizon to represent 100 Monte-Carlo years. The best computation times were obtained using the *CLARA* algorithm (a few seconds for one iteration of the algorithm), while the other algorithms were not suited for such large data sets as they present a quadratic complexity. Some of the selected snapshots can represent up to 90% of the 876,000 elements of the pool, while others only account for a few hundreds of snapshots.

Once the 45 representative snapshots were selected, we performed the candidate selection for each scenario and each time horizon. A first filter was applied on the 9,900 possible candidates to remove too long candidates (100 km for AC candidates and 1,000 km for DC candidates), leading to around 2,700 feasible candidates. Then, a relaxed TEP is run several times for each scenario and time horizon on the selected snapshots to detect which profitable candidates would be invested in. The obtained sets of candidates are merged into a unique one of 56 candidates. They are represented in Figure 22 (DC candidates are in red and AC candidates are in green). These candidates are the ones which would be the more beneficial for the system if they were invested in, considering the selected snapshots. Indeed, the operational savings they would bring are estimated over the representative snapshots, hence the importance of the snapshot selection.

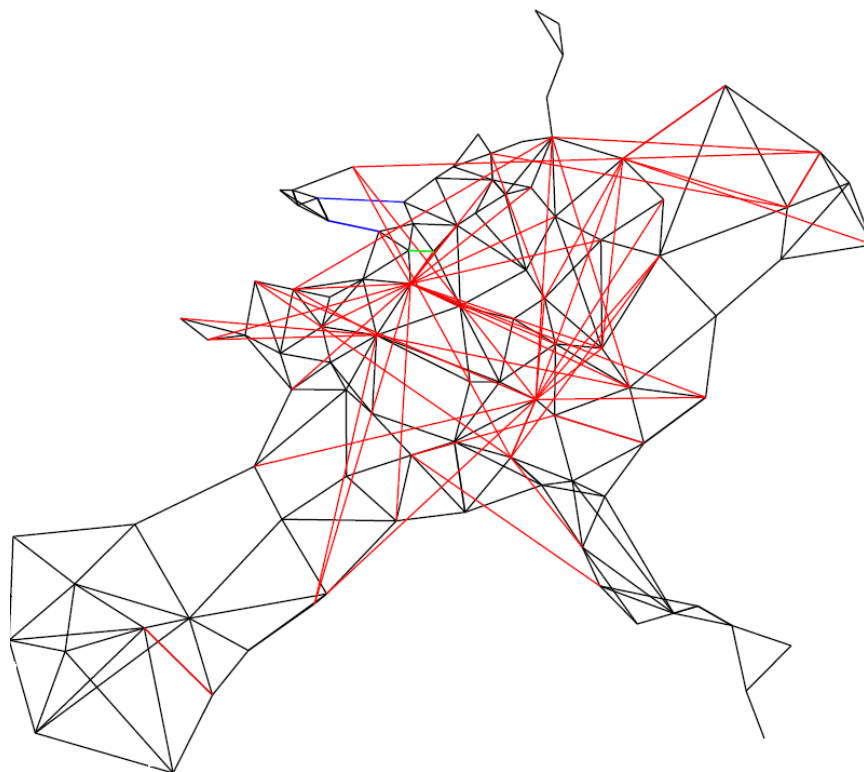


Figure 22 – Test case: 56 selected candidates (DC candidates in red and AC candidates in green; existing PST in blue)

At this stage of the methodology:

- the initial network has been reduced from 1,000 nodes to 100 zones, after a first simplification of the full initial grid (5155 nodes) to 1,000 nodes,
- the 900 Monte-Carlo years, i.e. the 7,884,000 simulated hours, are represented by only 45 snapshots, and
- the 9900 possible candidates for the zonal expansion have been reduced to 56 candidates.

The problem size has been drastically reduced using these temporal, spatial and stochastic reductions. Thus, this very complex problem becomes manageable by the transmission expansion planning, and can be solved within a reasonable time. In the test case, the TEP optimization is performed over 3 time horizons and for 3 different scenarios, with a common development of the grid for all scenarios in 2030. The modular development plan with the resulting grid architectures is illustrated in *Figure 23*.

Note. The presented results should be analyzed carefully: the input data used in this test case is not real data, but tries to be realistic. Thus, the obtained results should not be compared to the outputs of WP2, which conducted a serious study with real data.

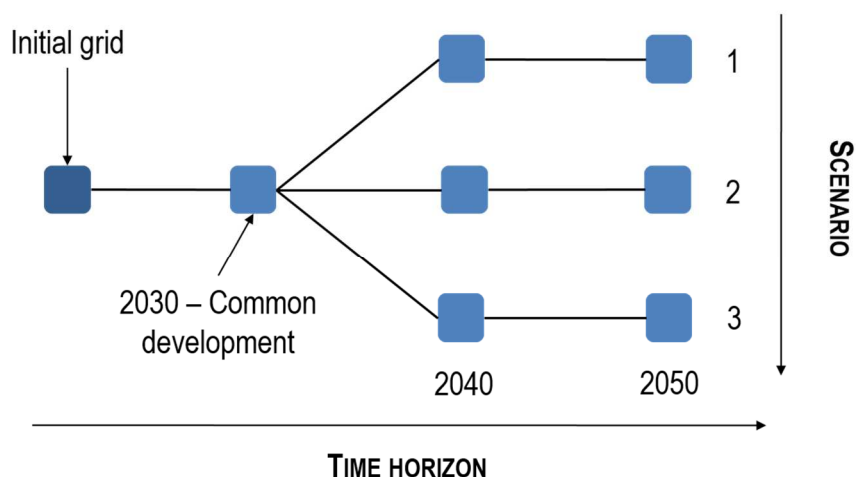


Figure 23 – Test case modular development plan: each square represents a grid architecture

The resulting grid architectures are represented in *Figure 24*, where invested candidates correspond to the red lines. In the first step of the modular development plan, 4 different candidates are installed in all scenarios, corresponding to 20 GW. Grid developments for each scenario considering all time horizons are also represented. We can notice that, in addition to the common developments of 2030, other investments appear in all scenarios.

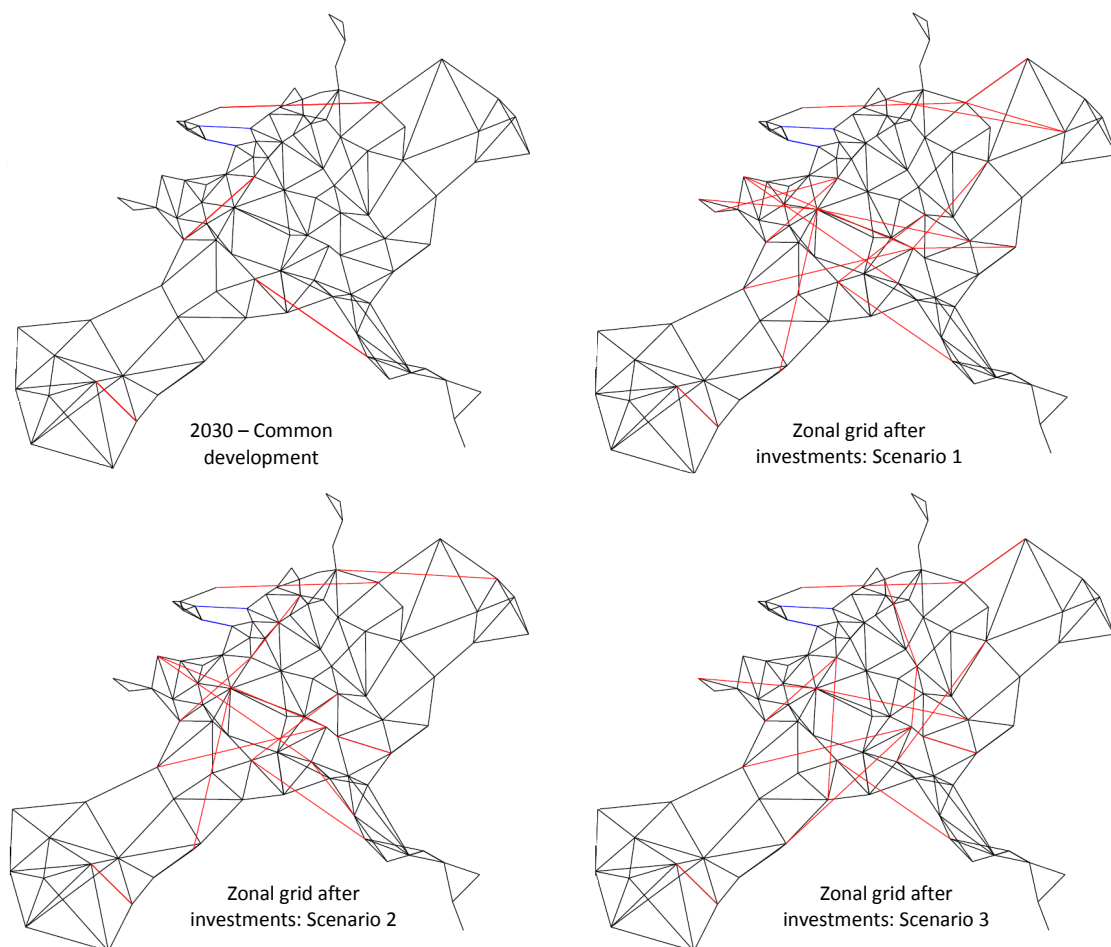


Figure 24 – Resulting zonal grid architectures after reinforcements: common development in 2030 (top-left) and all developments from 2030 to 2050 for scenario 1 (top-right), scenario 2 (bottom-left) and scenario 3 (bottom-right)

The detailed investments in GW for each scenario and time horizon are presented in *Table VII*, while *Figure 25* illustrates the cumulative installed transmission capacities. We can notice that the scenario with 100% RES generation in 2050 (Scenario 1) is the one requiring the most grid investments: indeed, this scenario relies even more on the transmission network to compensate the intermittency of its generation.

Table VII – Transmission grid investments (GW) for each scenario and each time horizon

| | 2030 – Common development | 2040 | 2050 | Total (GW) |
|-------------------|---------------------------|------|------|------------|
| Scenario 1 | | 48 | 12 | 80 |
| Scenario 2 | 20 | 12 | 32 | 64 |
| Scenario 3 | | 16 | 40 | 76 |

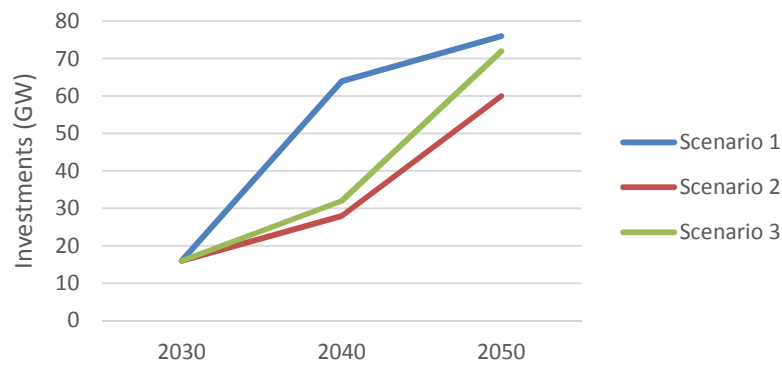


Figure 25 – Zonal TEP results: cumulative transmission grid investments in GW for each scenario

The resulting investment, operational and maintenance costs are represented in *Figure 26* for each scenario in 2050 relative to the cost obtained without grid investments, i.e. the total system cost with the initial grid. The operational costs are calculated over the selected snapshots. In all scenarios, the grid reinforcements enable huge savings compared to the situation with no investment. The sum of investment, operational and maintenance costs, i.e. the total cost after investment, represents less than 1% of the total system cost with no reinforcements. This large difference is mainly due to the load curtailment cost, whose cost was assumed very high (i.e. 10,000€/MW). Thus, the resulting zonal grid is a lot more profitable than the initial one. Indeed, the new grid architectures cope with issues of unsupplied energy (which is the main component of the operational cost with the initial grid), RES curtailment or generation redispatch. These results are also consistent with the installed transmission capacities: the benefits enabled by the grid reinforcements are the highest in Scenario 1 (with 100% RES generation), compared to the total system cost that would have been obtained if nothing were done.

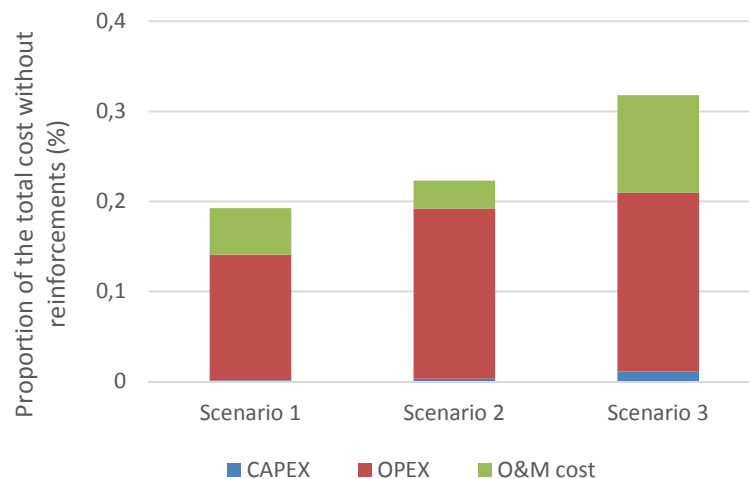


Figure 26 – Resulting costs relative to the total cost without grid investments

Grid investments are very dependent on the discount rate value. In the test case, we assumed a discount rate of 10%. Thus, it becomes a lot more interesting to invest in the grid in 2050 than in 2030. In order to force grid investments in the first horizon, we can set maximum investment constraints on the following horizons. However, these constraints increase the computation time of TEP optimization. Figure 27 illustrates the grid reinforcements obtained with tight investment constraints in 2040 and 2050. Consequently, most of the investments are made in 2030, while only a few candidates are installed in 2040 and 2050. We can notice that the resulting grid reinforcements are similar to the ones obtained in later horizons in Figure 24.

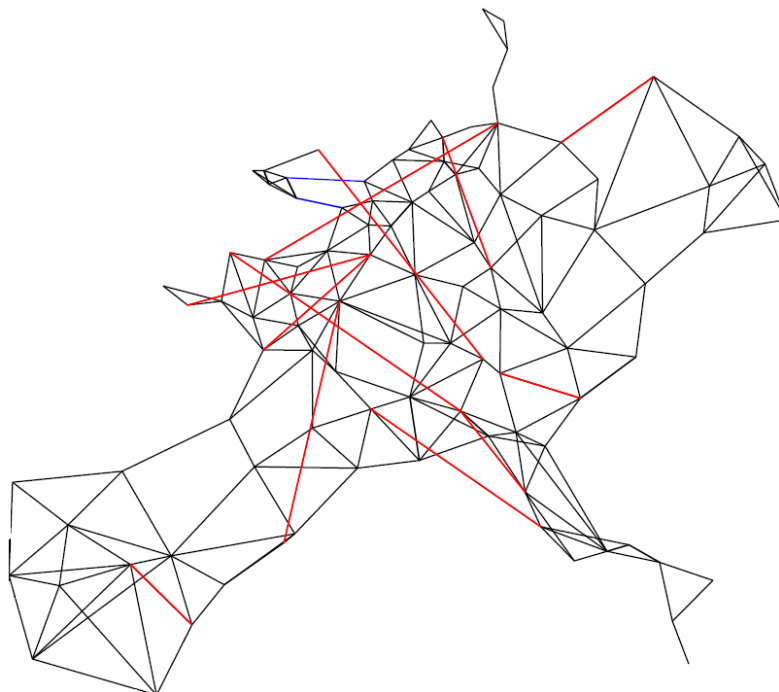


Figure 27 – Zonal grid architecture in 2030 after reinforcements, with a common development for all scenarios and investment constraints

The computation times for each step are presented in Table VIII. The zonal DCOPFs and the calculation of features are performed in parallel for each Monte-Carlo year, while the selection of snapshots (resp. candidates) is run over all the Monte-Carlo years (resp. selected snapshots) for each scenario and each horizon. Finally, the TEP optimization is computed on one server as the transmission expansion problem is optimized over all horizons and scenarios at the same time.

Table VIII – Computation times for the zonal transmission expansion planning

| | Average computation time for 1 year | Total computation time |
|---|-------------------------------------|------------------------|
| Zonal DCOPFs (total time for the 8760 hourly linear problems) | 40min | 4h |
| Zonal price differences calculation (average, min, max, standard deviation over the system) | 24min | 2h 20min |
| Snapshot selection (5 snapshots per scenario/horizon) | - | 30min |
| Candidate selection | - | 2h 27min |
| Zonal TEP optimization with 45 snapshots and 56 candidates | - | 2h |

6. Grid expansion at nodal level

The expansion at zonal level gives a solution in the form of equivalent physical capacities and reactances between zones for each scenario and time horizon. This is not a directly implementable expansion plan, which needs specific transmission lines with their corresponding end nodes, voltage levels and cable types. Therefore, one of the tasks in the proposed methodology is precisely the determination of the nodal expansion plan for time horizons, for which there is a common zonal expansion plan for all scenarios.

However, the complexities of the power system make it impossible to translate the resulting zonal expansion into an equivalent nodal expansion with identical results for system operation. This task aims at matching them as accurately as possible. Moreover, the obtained nodal expansion plan should ensure system reliability (N-1) taking into account all possible flexible devices, while N-1 contingencies were not considered in the former steps.

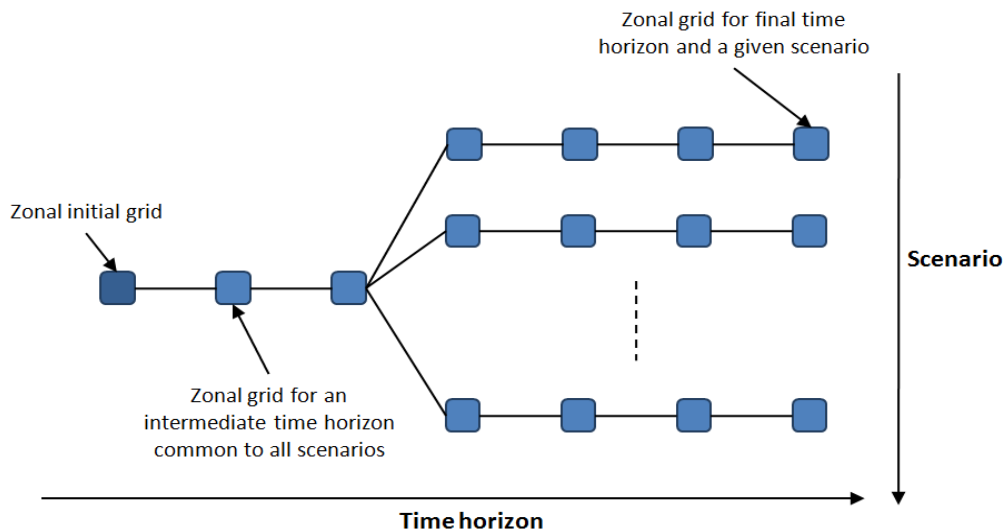


Figure 28 - Representation of the expanded network solutions

In order to perform the transmission expansion of the network at the nodal level, we use the model TEPES (Transmission Expansion Planning for an Electric System), developed by Comillas. A more detailed description of TEPES can be found in reference [17] and in deliverable 8.3a [7].

6.1. Identification of transmission investment candidates

Similar to the zonal expansion problem, taking into account all possible transmission investments is impossible due to the enormous number of combinations that could be considered. Even though, the combinatorial problem is even higher in the nodal expansion because the network is much more detailed than in the zonal one. Furthermore, it is also necessary to take into account the modular development plan previously determined in the zonal expansion, so that the network expansion obtained at the nodal level is coherent with the zonal expansion plan.

Thus, in order to be able to solve the nodal expansion of the grid, it is necessary to reduce the number of possible candidate investments. We have two types of candidates that must be considered:

- The lines that allow complying with the zonal expansion previously determined over the whole set of scenarios and time horizons.

- The most promising investments only considering the first time horizons.

In order to select the most promising investment candidates to be considered, we propose to use the work presented in [16] and that is also described in deliverable 8.3a [7]. This method selects the most promising candidates to be installed based on the potential benefits that are brought by each candidate line. These potential benefits are approximated as the congestion rent that would be perceived by the transmission line in a hypothetical case where its inclusion did not produce any modifications on system operation. This approximation will generally be higher than the real impact of the line as the nodal prices at the extremes of the transmission line will tend to be closer once a line between them has been installed.

The candidate lines that will allow complying with the final capacities determined in the zonal expansion could not be included in the most promising ones (maybe they will be profitable in the next time horizons). The most promising candidates are defined by only considering the first time horizons, while the zonal investments take the future into account. Thus, some zonal investments made during the first time horizons may not appear to be profitable if the future is not considered, that is why some candidates may not be in the most promising pool. Therefore, we have established that a minimum number of candidate lines should be proposed in order to meet the inter-zonal capacities determined in the zonal plan. For instance, we assumed that the total capacity of these candidates should be 20 times higher than the zonal invested capacity in the test case. It is important that this set of candidate lines is big enough so that the TEPES model has a variety to choose the most interesting ones to be installed.

6.1.1. Types of transmission investments considered

In order to compute the optimal expansion of the network, different technologies for the transmission investment candidates can be considered:

- HVAC transmission lines and transformers.
- HVDC transmission lines and converters.
- Phase-shift transformers (PST).

Regarding the modelling of the flow of power in the network, the first Kirchhoff law (transportation model) has been considered for DC lines and converters and the first and second Kirchhoff laws (DC model) for AC lines. PSTs are modelled using only the first Kirchhoff law.

It is also important to remark that the TEPES model not only decides to install a candidate line or not, but it also decides if several circuits of the same candidate line could be installed in parallel. This second option can be interesting to face N-1 issues.

6.2. Transmission expansion at nodal level

The transmission network expansion is based on the joint minimization of network investment and network and system operation costs. Network investment and operation costs refer to the costs of building the infrastructures (transmission lines or converter stations) and the costs to operate and maintain this piece of infrastructure. Meanwhile, system operation costs refer to the costs related to the generation of energy by power plants. This process is carried out with the TEPES Model, which minimizes total network investment and operational costs subject to a set of constraints that represent node energy balances, line flow capacity limits and others.

The operation of the system (generation and demand) has been represented using a set of snapshots that try to represent the situations that may develop over the whole target year. These snapshots are the same snapshots selected for the network expansion at the zonal level, but only the ones that belong to the first time horizon are considered. The model selects the candidates that should be built to minimize total costs (investment plus operation) while complying with boundary constraints.

Investment decisions affecting individual network assets, like AC lines, transformers, offshore lines, etc., are discrete, i.e. only a discrete number of units of this asset can be built. Nonetheless, the model provides the user with the option of deciding if investments are continuous or discrete. Discrete investments are more accurate and realistic, but the problem becomes more computationally demanding.

TEPES is implemented in GAMS and can be solved using different solvers (CPLEX, GUROBI). The interface receives data and provides results in Microsoft Excel spreadsheets. In addition, the tool is integrated with Google Earth to provide easy visual inspection of results.

6.2.1. Considering system reliability

TEPES can consider reliability as a partial objective. This is carried out by including stochastic scenarios that describe either generation or transmission contingencies. However, given the size of the nodal network and the number of candidates to be considered, taking into account the full set of contingencies is not possible. Hence, we propose:

- Particularly important elements, such as HVDC lines, are considered explicitly.
- The reliability of other transmission lines is considered implicitly by means of imposing redundancy constraints to the transmission lines added to the grid. This redundancy is established to limit the capacity that is lost if one line fails, and follows the heuristic defined in reference [18].

This heuristic assumes that there is a pre-existing line of capacity C_0 . The expansion plan will add n new lines of capacity C . Because of reliability reasons, the flow is limited to a maximum proportion of capacity p . We can use the table below for determining the most appropriate overlays depending on the proportion of flow that we consider.

Table IX – Maximum proportion between the capacity of the reinforcements and the original one depending on the proportion of flow allowed and the number of corridors added

| p | n | Maximum C/C_0 |
|------|-----|-----------------|
| 0,7 | 1 | 0,429 |
| 0,7 | 2 | 0,75 |
| 0,7 | 3 | 3 |
| 0,75 | 1 | 0,33 |
| 0,75 | 2 | 0,5 |
| 0,75 | 3 | 1 |
| 0,8 | 1 | 0,25 |
| 0,8 | 2 | 0,33 |
| 0,8 | 3 | 0,5 |
| 0,9 | 1 | 0,111 |
| 0,9 | 2 | 0,125 |
| 0,9 | 3 | 0,143 |

6.3. Test case results

The original network considered in this step is the network depicted in Figure 3 and its characteristics are listed in Table III. The modular development plan requirements determined in the zonal expansion are indicated in Table XIV: they correspond to the common investments for 2030. Each line is defined by two end zones: Zone A and Zone B.

Table X – Zonal expansion plan requirements for the first time horizon (2030)

| Number of Zone A | Number of Zone B | Installed capacity [MW] |
|------------------|------------------|-------------------------|
| 9 | 19 | 4,000 |
| 77 | 78 | 4,000 |
| 54 | 96 | 4,000 |
| 57 | 59 | 8,000 |
| Total | | 20,000 |

On one hand, we have established that the candidates included in order to comply with these requirements should amount for a total capacity 20 times higher than the total capacity required. Then, the total number of candidates included with this purpose is 110. On the other hand, the number of candidates selected due to be promising investments are 297. Thus, we are considering a total number of candidates of 407.

As previously explained, the snapshots considered for the nodal expansion are the same snapshots considered in the zonal expansion. However, in this step we are only considering the corresponding snapshots to the first time horizon (2030). Thus, we have 15 snapshots: 5 for each scenario.

The nodal expansion could be performed using continuous or discrete variables for the investment decision on the candidate lines and PSTs. Of course, the use of discrete variables produce more accurate and realistic results, while increasing the computational time.

The nodal expansion is performed using the TEPES model under a Windows Server 2012 R2 with 20 cores 2,60Ghz and 144GB of RAM.

6.3.1. Continuous variables

This section presents the results obtained when using continuous variables for the investment decisions. The main characteristics of the nodal expansion plan obtained are displayed in Table XI.

When analysing the results, it is interesting to notice that only nine of the investment decisions made are not discrete.

Table XI – Main characteristics of the nodal expansion plan obtained using continuous variables

| | |
|---|-------------------------|
| Investment cost | 11,346 M€/y |
| Operational cost | 75,741 M€/y |
| Energy Not Served | 0 GWh |
| Capacity built | 20.65 GW |
| Capacity built * Distance | 16,504 GW * Km |
| Number of investments | 114 (28% of candidates) |
| Optimality gap | 0.26% |
| Computational time (CPU time) | 144 seconds |
| Total time (including processing of data and results ⁴) | 586 seconds |

6.3.2. Discrete variables

This section presents the results obtained when using binary variables for the investment decisions. The main characteristics of the nodal expansion plan obtained are displayed in Table XII.

Table XII – Main characteristics of the nodal expansion plan obtained using discrete variables.

| | |
|---|-------------------------|
| Investment cost | 11,269 M€/y |
| Operational cost | 76,021 M€/y |
| Energy Not Served | 0 GWh |
| Capacity built | 21.7 GW |
| Capacity built * Distance | 16,499 GW * Km |
| Number of investments | 111 (27% of candidates) |
| Optimality gap | 0.30% |
| Computational time (CPU time) | 512 seconds |
| Total time (including processing of data and results) | 1,268 seconds |

When analysing the results, it is interesting to notice that a high number of the investment decisions made are the same than in the case when continuous investment variables are employed: 102 of the investment decisions are exactly the same. However, there are some little differences. On one hand, there are some lines that were previously installed, at some level, and that now are not being installed. On the other hand, there are also new installations when comparing to the case when using continuous investment variables.

⁴ This time includes the input and output of data from Excel files.

7. Robustness of the proposed architectures

DC load flow models are widely used for electric power systems analysis, since it is linear and thus easy to implement in other procedures. In addition, the linearized DC model is especially useful when the network data is incomplete. Previous tasks of this work package (WP8) have been using the linearized DC model.

However, a full AC model of the network may be required to carry out more complex analyses, such as transient stability, N-1 voltage constraints, etc. Therefore, the first objective is to build an AC load flow model from the DC load flow one. The construction of the AC load flow model involves the dispatch of voltage-reactive power control resources (shunt devices, transformer taps and generator set point voltages).

The robustness analysis involves the study of voltage-reactive power control and stability, transient stability and small-signal stability. These three stability issues are of different time scales. Voltage stability is analysed by means of steady-state models and AC load flow tools. Transient and small signal stability analyses require dynamic models as well. Transient stability is analysed through time-domain simulations, whereas small signal stability is analysed through eigenvalue analysis. Automatic building procedures of both steady-state AC load flow models and dynamic models have been developed.

Figure 29 shows an overview of the procedure of the robustness analysis. This analysis starts by building an AC load flow model from the DC load flow model used for grid expansion purposes. The AC load flow model is directly used to assess voltage stability in terms of voltage collapse. For transient and small signal stability analyses, a dynamic model needs to be built, employing standard generation technologies. Transient stability is assessed in terms of critical clearing times to three-phase bus faults, whereas small signal stability is measured by means of eigenvalues and participation factors. The robustness analysis pinpoints effective control and protection actions.

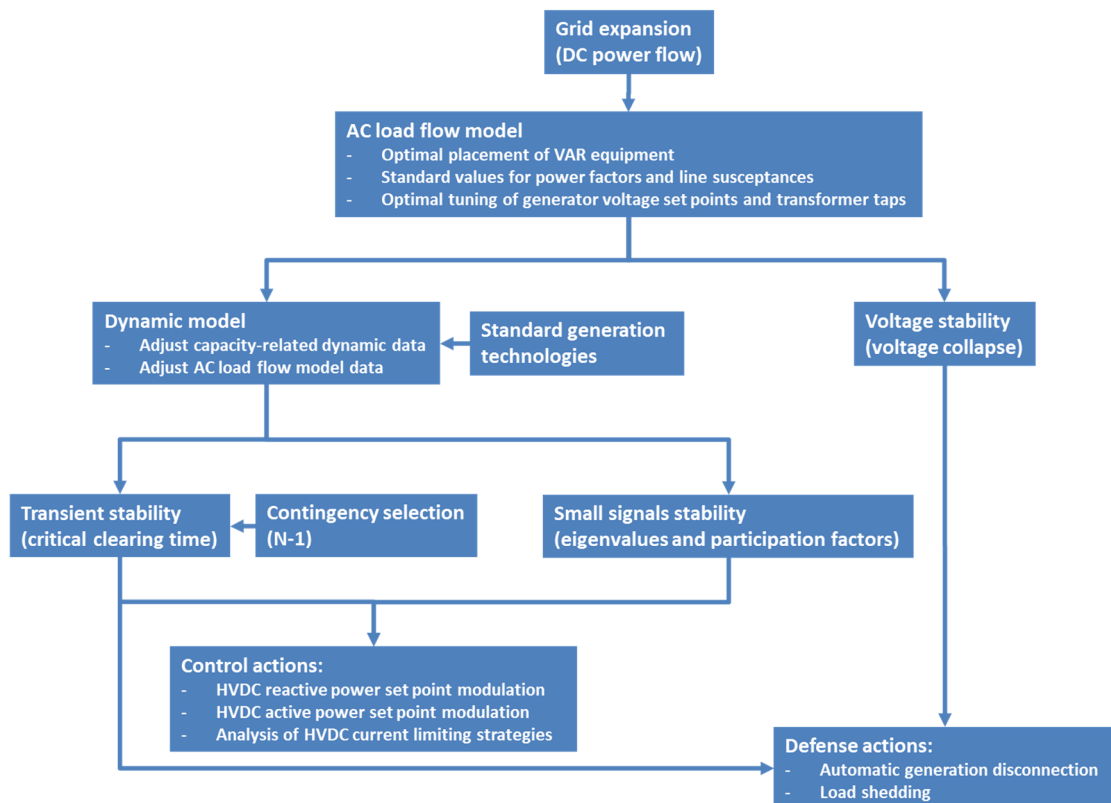


Figure 29 – Overview of the procedure of the robustness analysis

7.1. DC-to-AC procedure

The DC-to-AC procedure dispatches voltage-reactive power control resources to attain AC load flow within an admissible voltage range [9]. However, the main issue of this method was the convergence of the initial load flow which could occur in a planning study and does not occur on actual realized data. The DC load flow model does not account for (active power) losses. Hence, losses must be estimated to incorporate generation to supply losses in order to avoid that losses are only supplied by the swing bus in the AC load flow solution. If losses were to be supplied by the swing bus, power flow of branches close to the swing bus might be distorted.

The branch data in the DC load flow data set contains branch resistance and reactance. Transmission line data includes line length. The total line susceptance is computed using pu/length susceptance with data of standard overhead lines. The line length is determined from the actual line reactance and the pu/length reactance of a standard overhead line.

The computation of the AC load flow solution also requires reactive power consumption of the loads (load power factor) and reactive power capability (both maximum generation and consumption capability) of generators. Therefore, load power factor and generator reactive power capability are parameters that have to be set by the user.

The issue of the procedure is the convergence of the initial load flow. Considering the fact that the initial version of the AC model has every reactive power control device in flat mode, divergence of the load flow calculation is likely to occur. If the initial AC load flow does not converge, a new algorithm has been proposed and implemented. If a divergent load flow problem occurs, a sequential combination of a non-divergent load flow algorithm and a sensitivity algorithm is used. Therefore, once a minimum mismatches solution has been found, sensitivities are used to identify optimum location for shunt devices that will improve the convergence of the case scenario.

During DC-to-AC procedure development, some numeric issues have appeared. These numeric issues are related with the fact that DC power flow is linear, thus some magnitudes may not be troubling since no convergence process is considered:

- **Active power system balance:** Power balance is a key variable to guarantee the convergence of the power flow. The sum of the active power production has to be equal to the demand plus the active power losses. Thus, a great unbalance between power generation and demand will lead to a divergent power flow.
- **Active power system inter-zone balance:** The inter-zone power exchanges are defined by the difference between the generation and the demand in the zone. Great unbalance between interconnected zones may not only complicate the convergence, but the final case scenario will probably present unrealistic inter-zone power transfers.
- **Line parameters:** In network planning using reduced networks, some lines can be defined using unrealistic parameters of lines that may lead to power flow divergence. Most common unrealistic parameters are related to the length of the lines: low impedance lines (typically $z < 1.0e-4$ pu, equivalent to 500 m of a 380 kV line) and high impedance lines (typically $> 2.0e-1$ pu, equivalent to 1000 km of a 380 kV line). Both of them add noise to the power flow solution and make the convergence procedure more difficult.

7.2. Voltages stability assessment

Voltage stability is becoming one of the most important issues in the power systems due to the intensive use of the transmission networks. Voltage stability is concerned with the ability of a power system to maintain acceptable bus voltages under normal conditions and after being subjected to a disturbance. The accurate representation of the voltage instability phenomena requires a detailed model of power system components (generators, transformers, loads, etc.). The risk of voltage instability of a power system can be measured by the distance of the steady-state power flow equations from the initial point of operation (base case) to its saddle node bifurcation point, known as the voltage collapse point. This distance is usually called stability margin. Therefore the voltage collapse point will correspond to the solution of the optimization problem which maximizes the load factor subject to power flow equations, and its solution not only satisfies power flow equations, but also implies the singularity of the Jacobian.

The method selected to compute the voltages collapse point belongs to the continuation techniques family, thus the state variables manifolds from starting point to voltages collapse may be drawn [10]. Precisely, the technique selected is a binary search where for each increment in the power dispatch control parameter, the corresponding solution is attempted to be obtained. If a solution exists, it saves the point and applies another power dispatch control parameter. If the power flow is unfeasible for that power dispatch control parameter, the step is reduced. The process is considered finished when a minimum step is reached while the power dispatch control parameter is getting higher. A flow chart of the procedure is depicted in **Figure 30**.

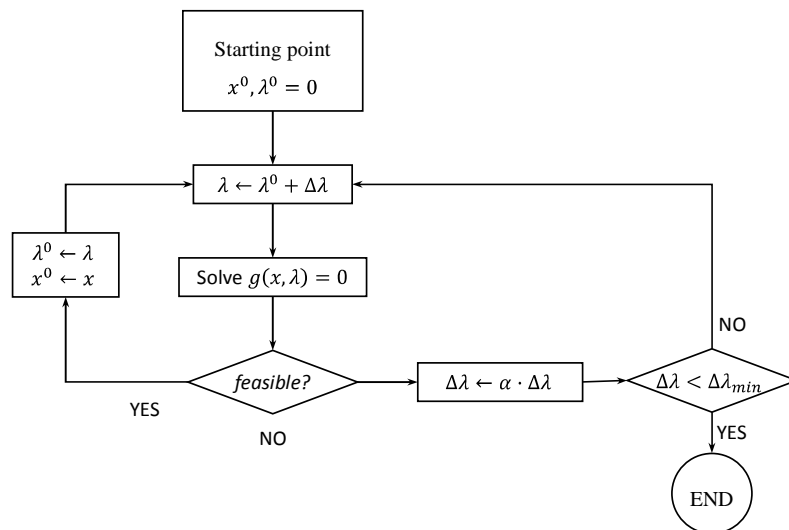


Figure 30 – Flowchart of the computational procedure to determine the point of voltage collapse

7.3. Transient stability

This section presents the methodology developed for the analysis of transient stability of electrical power systems.

The transient stability of a power system is measured by the critical clearing times of faults, i.e. the maximum duration of the fault for which the power system does not turn unstable. A system turns unstable when the relative angles after clearing the fault do not return to their initial values but instead continue diverging. If one relative angle exceeds a previously determined critical angle, the system is deemed unstable and the critical clearing time exceeded. Critical clearing times below times of protections either affect the design of the grid or require special protection schemes (defence plans).

Transient stability analyses not only need the steady-state model of the network provided by an AC load flow, but also the dynamic model of generators and other dynamic devices. Generating units have been classified according to six generation technologies: nuclear, thermal, combined cycle, gas, hydroelectric and RES power plants. For each generator technology, the model components have been identified and an existing power plant with known model parameters has been used as a reference plant. The resulting models are referred to as *standard models*.

Figure 31 provides an overview of the procedure to build the dynamic model of the system. The dynamic model builder essentially reads a converged AC load flow file and particularly the generator data, and assigns to each generator a corresponding, standardized dynamic model based on its inherent technology (e.g., nuclear or hydro generation).

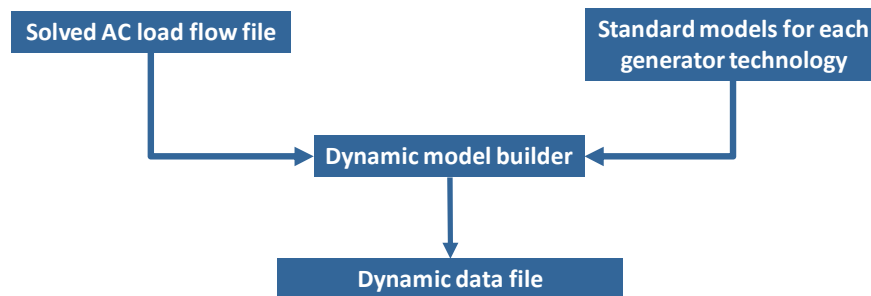


Figure 31 – Overview of the procedure to build the dynamic model of the system

In addition to synchronous generators models, RES generating units and HVDC links have been built and analysed to cope with expectable generation and grid expansion scenarios in the short term. It has been found that over simplified models of RES generators should be avoided for providing optimistic results in terms of critical clearing time of a small-scale test system.

Figure 32 provides an overview for the calculation of the critical clearing time of a fault. For a given fault, the fault is applied for a certain duration and subsequently removed. The dynamic response of the power system to the fault and particularly, the responses of generators in terms of relative angles are simulated. If one relative angle is larger than the critical angle, the system is deemed unstable and the previously applied duration is the critical clearing time. Otherwise, the process is repeated until a critical clearing time is found.

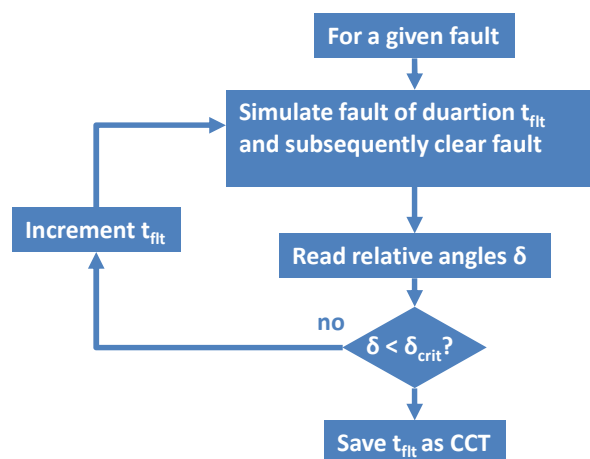


Figure 32 – Overview of the critical clearing time calculation

Finally, it is worthwhile to mention that some controls contribute to improve the transient stability of the small-scale power system, whereas other controls deteriorate it. After all, reactive power and voltage

controls have been analysed to this regard. According to whether additional RES generators or the HVDC link terminals are located in an importing or exporting area, reactive power control can be more beneficial than AC-voltage control. However, it is of importance that these controls are analysed for each case and particularly for varying system operating conditions affecting inter-area flows, etc.

7.4. Small signal stability

This section presents the methodology and tools developed for the analysis of small signal stability of electrical power systems. Small-signal stability looks at the damping of the electromechanical oscillations of synchronous generators. Should the damping of electromechanical oscillations be below a safe value, power system stabilizer of generators must be redesigned.

Software packages such as PSS/E provide additional modules to evaluate small signal stability of a power system. NEVA is such a module, offering QR method and selective modal analysis. However, NEVA only is able to analyze some of the PSS/E dynamic library models. VSC HVDC links or wind power generation models cannot be analyzed. Further, user defined models are not supported either. A Matlab-based tool SSST has been therefore developed to study small signal stability. The main functions of SSST are: load flow solution, output of load flow solution, linear model, eigenvalue analysis, output of the eigenvalue analysis, linear responses, and reduced order eigenvalue analysis.

7.4.1. Data format conversion

In a first step and in order to guarantee interoperability with PSS/E used for transient stability analysis, the PSS/E data format needs to be translated into the SSST format. This format translation is illustrated in **Figure 33**. Two input files are required: an AC or AC/DC load flow file (.lfd) and a dynamic data file (.dyd).

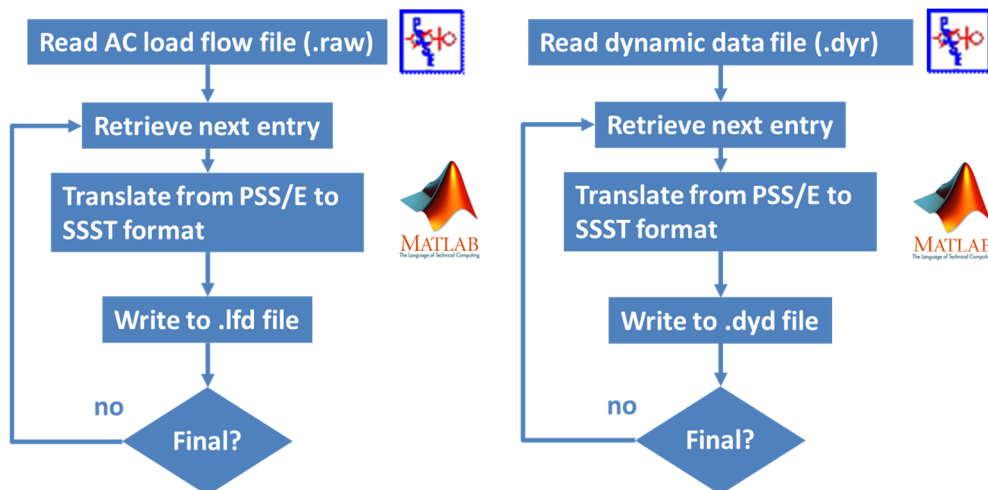


Figure 33 – Translation from PSS/E to SSST data format

The data format for AC and AC/DC load flow input files including VSC-HVDC links and the data format for dynamic input files is described in the Appendix.

Whereas models for excitation systems, governor systems and generators are standard library models, which have been described in [10], the VSC-HVDC link model is not a library model. **Figure 34** shows the converter model and its connection to the AC and the DC grid. This model is an extended version of the one used for PSS/E studies by modeling coupling transformers and filters too. Further, the DC link is dynamically modelled contrary to the VSC-HVDC model of PSS/E.

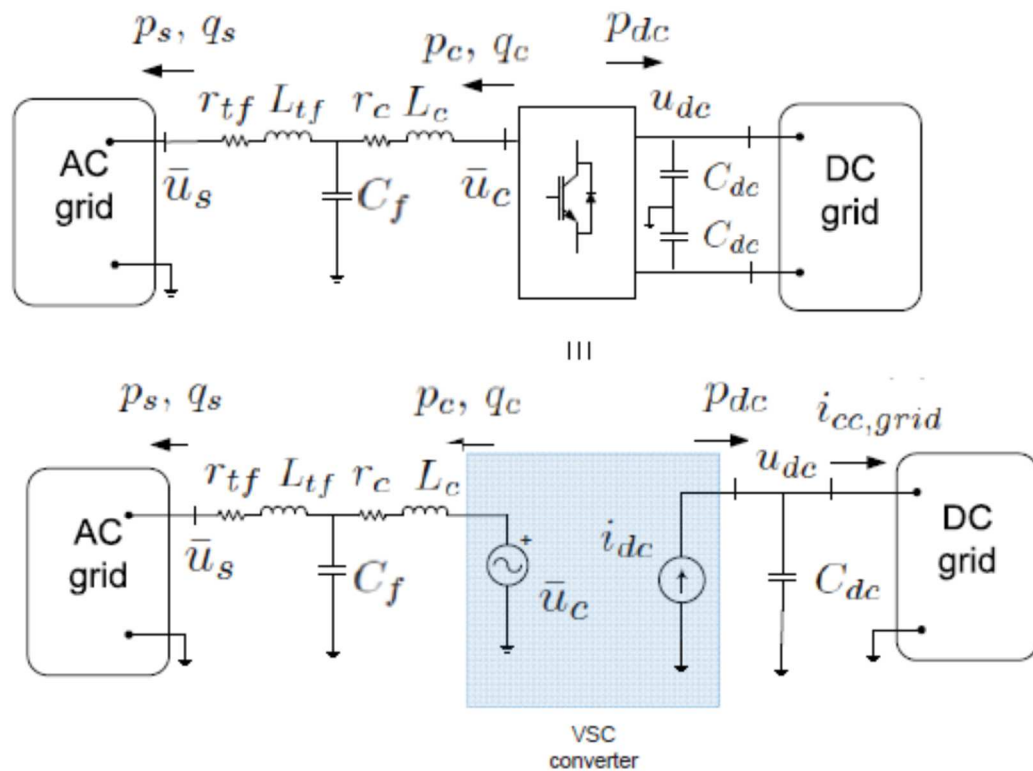


Figure 34 – HVDC link model [21]

The VSC converter control comprises two loops: an inner dq -axes current control loops, approximated by first-order lag models, and external active power/dc-link voltage and reactive power/AC voltage controllers. These external controllers are modelled as PI controllers [21].

7.4.2. Eigenvalue analysis

Second, eigenvalues of the power system need to be evaluated in order to assess small signal stability. A positive real eigenvalue or a complex eigenvalue with positive real part are tantamount to small signal instability.

Eigenvalue analysis requires a linear system of dynamic equations. The SSST tool builds the linear model of a power system in implicit form. The implicit form of the system model comprises the matrices of the state space representation of the dynamic devices (generators, HVDC links, FACTS, etc.) and the admittance matrix expanded to its real and imaginary parts including the representation of the nonlinear loads. First, the implicit model of the individual power system components are obtained. Second, the power system model is determined by assembling the power system components.

Once the linear model is available, the tool computes the eigenvalues as well as the right and left eigenvectors. For smaller systems, the QR method can be directly used, determining all eigenvalues. The right eigenvectors may be computed by using the inverse iteration technique. A good description of the QR transformation and inverse iteration methods may be found in [23]. Right and left eigenvectors can be used to define the participation factors, indicating to what extent a particular state variable contributes to a certain mode (eigenvalue). Right and left eigenvectors are also used to compute controllability and observability factor, respectively. Finally, the right eigenvectors provides the mode shape.

For very large power systems, the tool includes selective modal analysis and the modified Arnoldi method. Selective Modal Analysis (SMA) is a comprehensive method for the characterization and analysis of selected parts of the linear time invariant dynamic systems. SMA contains sensitivity tools to identify the relationships between state variables and modes and reduced order eigenvalue analysis methods to determine few selected modes. The SMA sensitivity measures are the participation factors. **Figure 35** shows an overview of the eigenvalue analysis.

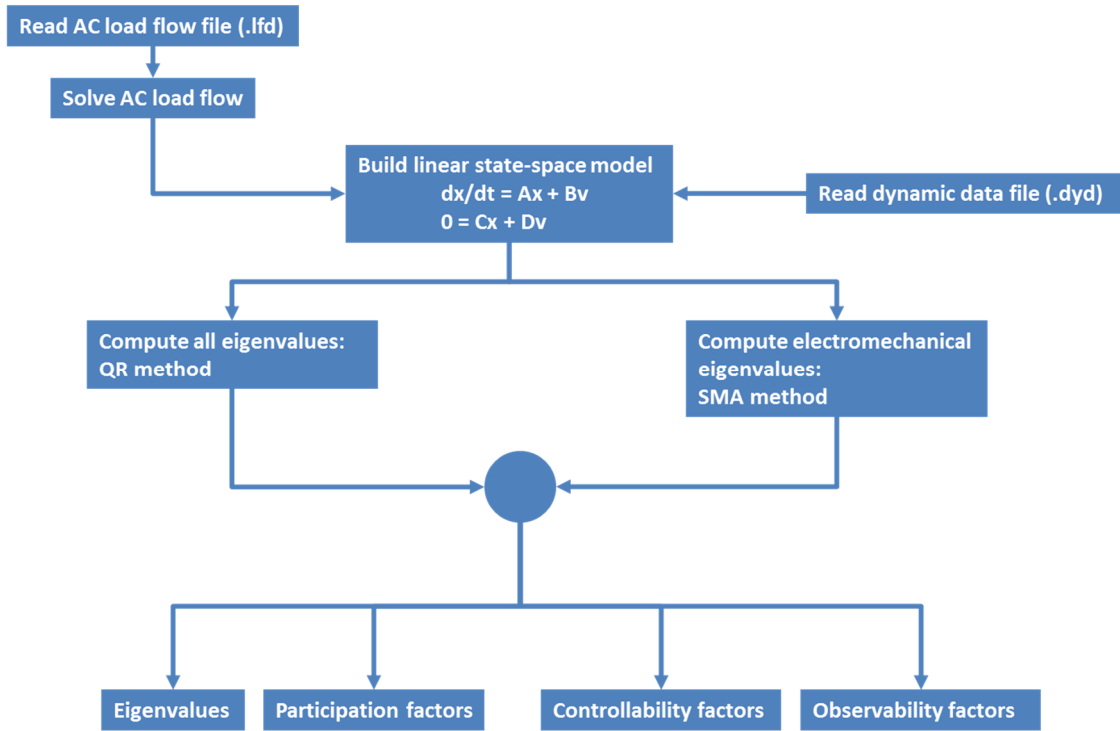


Figure 35 – Eigenvalue analysis

7.4.3. SSST validation

In order to validate the toolbox and its applicability to AC systems with HVDC links, the results in terms of eigenvalues of the SSST have been compared with the results of the eigenvalue analysis provided by PowerFactory.

For this purpose, a simple test system has been analysed. **Figure 36** shows the single line diagram of the test system.

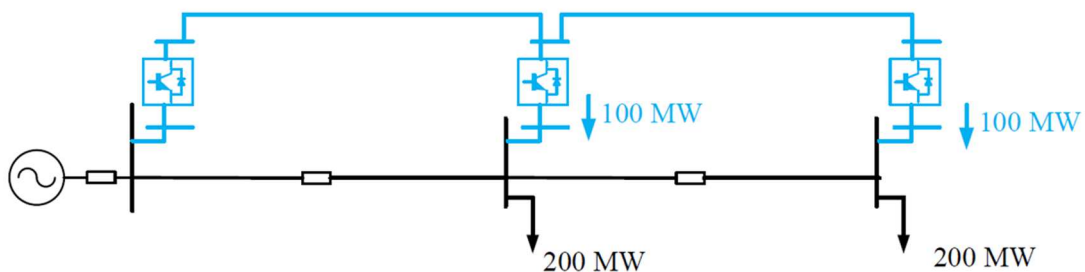


Figure 36 – Single line diagram of the test system to compare SSST and PowerFactory

The following table compares the eigenvalues obtained either by SSST or by PowerFactory. Only those eigenvalues common to both are shown. In fact, PowerFactory exhibits additional eigenvalues related to PLLs

and DC link modeling. The description of the latter with PowerFactory documentation is not conclusive. It can be seen that complex eigenvalues are slightly different but within the same order of magnitude, whereas real eigenvalues are about the same.

Table XIII – Comparison of eigenvalues obtained either by SSST or PowerFactory

| Mode | Eigenvalues | | | |
|------|-------------|-----------|--------------|-----------|
| | SSST | | PowerFactory | |
| | Real | Imag | Real | Imag |
| 3 | -11.5303 | 1092.0894 | -15.3611 | 1092.2866 |
| 4 | -66.6972 | 661.6394 | -70.4165 | 660.9082 |
| 5 | -29.2193 | | -24.6866 | |
| 6 | -87.8927 | | -106.7062 | |
| 7 | -303.6779 | | -296.7873 | |
| 8 | -500.5595 | | -500.0641 | |
| 9 | -500 | | -500 | |
| 10 | -500 | | -500 | |
| 11 | -500 | | -500 | |
| 12 | -505.8319 | | -504.2078 | |

7.4.4. Reduced size illustrative example

A reduced size, 24 clusters model of the French-Spanish-Portuguese power system is used to illustrate the eigenvalue analysis [9]. **Figure 37** shows the 24-cluster model with two VSC-HVDC link between Spain and France.

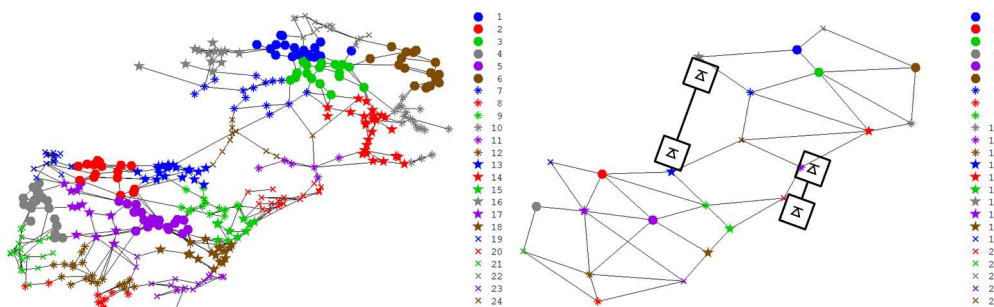


Figure 37 – 24 cluster model with two VSC-HVDC links.

The eigenvalues with and without the VSC-HVDC links are analysed. **Figure 38** shows all eigenvalues of the 24 cluster model without HVDC links. The system is stable. The least damped electromechanical mode has a damping of 2.16 % and a frequency of 1.57 Hz. **Figure 39** depicts the electromechanical modes only. A 5%-damping limit is also shown.

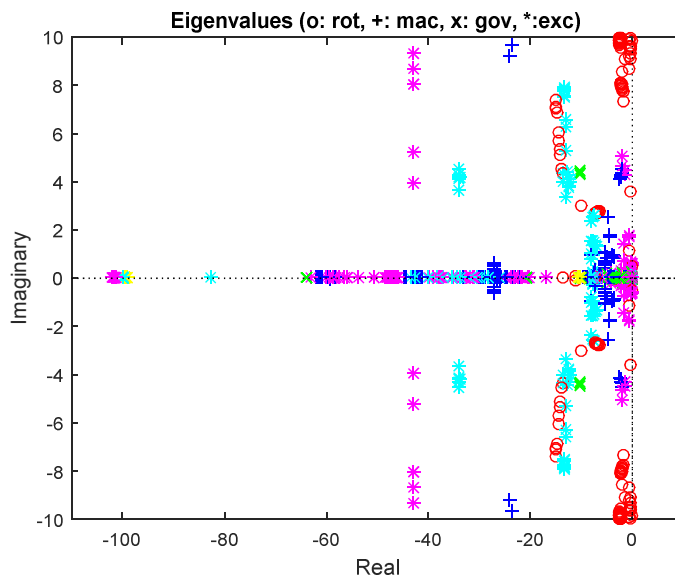


Figure 38 – Eigenvalues of the 24 cluster model without HVDC links

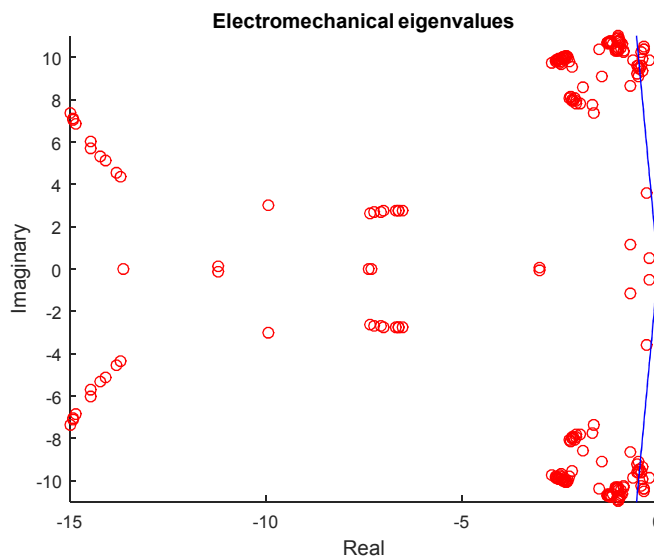


Figure 39 – Electromechanical eigenvalues of the 24 cluster model without HVDC links

Figure 40 depicts the electromechanical modes of the 24 cluster model with HVDC links. The system is stable. Like in the case without HVDC links, the least damped electromechanical mode has a damping of 2.16 % and a frequency of 1.57 Hz. Comparing Figure 39 and **Figure 40** suggests then that the HVDC links hardly affect the electromechanical oscillations. This is also confirmed in **Figure 41**, which compares the damping of the electromechanical modes.

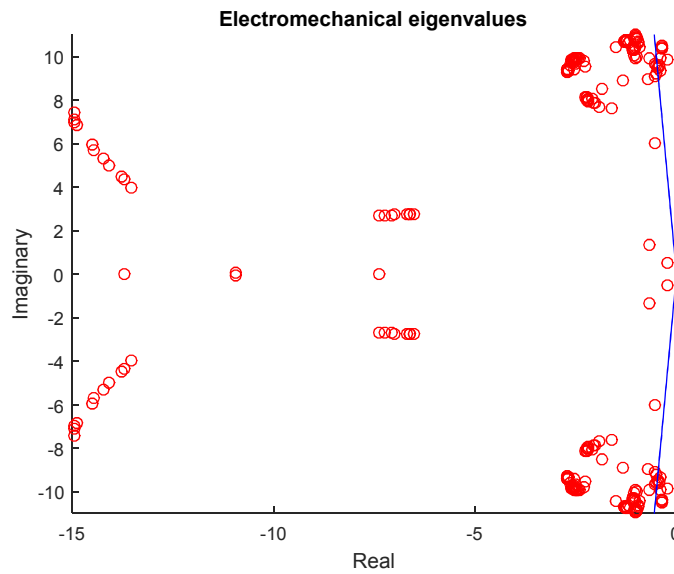


Figure 40 – Electromechanical eigenvalues of the 24 cluster model with HVDC links.

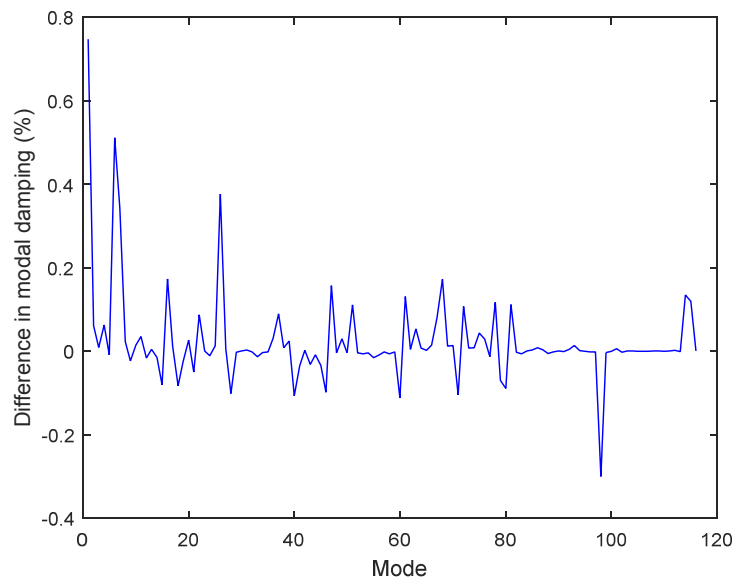


Figure 41 – Comparison of the electromechanical eigenvalues of the 24 cluster model in terms of the difference of modal damping with and without HVDC links.

7.5. Test case results

This section presents results on the full AC power flow model built. These results are power balance of the scenario and voltages report. In addition, results on voltages stability, such as critical load margin and nose curves are included.

7.5.1. Case scenario description

Table XIV and Table XV represent active and reactive power balance respectively. The power balance has been reported by areas and the total.

Table XIV – Active power balance

| area | FROM | TO | | |
|---------|----------|----------|--------|----------|
| | GEN | DEMAND | LOSSES | EXPORT |
| AREA AT | 13558.2 | 12606.4 | 81.6 | 870.2 |
| AREA BE | 12481.8 | 14390.6 | 26.7 | -1935.6 |
| AREA CH | 15035.7 | 10973.7 | 68.8 | 3993.1 |
| AREA CZ | 14342.8 | 9998.7 | 161.8 | 4182.3 |
| AREA DE | 69404.7 | 84176.2 | 895.5 | -15667.0 |
| AREA DK | 2878.3 | 2335.0 | 3.1 | 540.2 |
| AREA ES | 48930.4 | 41781.8 | 372.1 | 6776.5 |
| AREA FR | 80482.7 | 76850.1 | 970.4 | 2662.3 |
| AREA GB | 11096.4 | 10933.0 | 163.4 | 0.0 |
| AREA IT | 49448.6 | 53948.6 | 814.7 | -5314.6 |
| AREA NL | 19375.8 | 18701.8 | 106.9 | 567.2 |
| AREA PL | 28425.2 | 23914.9 | 201.3 | 4308.9 |
| AREA PT | 6321.6 | 8622.0 | 65.6 | -2366.0 |
| AREA SI | 3570.0 | 2167.0 | 20.4 | 1382.6 |
| TOTAL | 375352.1 | 371399.8 | 3952.4 | |

Table XV – Reactive power balance

| area | FROM | | | TO | | |
|---------|---------|---------|----------|----------|---------|--------|
| | GEN | SHUNT | LINES | DEMAND | LOSSES | EXPORT |
| AREA AT | 3958.3 | 0.0 | 1955.6 | 4253.2 | 1974.5 | -313.7 |
| AREA BE | 2808.9 | 0.0 | 3428.1 | 4949.7 | 1371.5 | -84.2 |
| AREA CH | 2880.6 | 0.0 | 2497.8 | 3611.3 | 1919.6 | -152.5 |
| AREA CZ | 1740.8 | -83.4 | 4261.3 | 3383.8 | 3028.5 | -493.6 |
| AREA DE | 18694.4 | -2698.0 | 29795.8 | 30036.1 | 15210.9 | 545.1 |
| AREA DK | 405.7 | 0.0 | 618.0 | 1117.9 | 290.5 | -384.6 |
| AREA ES | 5680.1 | 995.1 | 15854.8 | 15233.2 | 7640.9 | -344.2 |
| AREA FR | 7358.3 | 2998.2 | 34455.0 | 26827.5 | 16243.3 | 1740.8 |
| AREA GB | 1449.5 | -965.2 | 7670.8 | 4532.9 | 3622.3 | 0 |
| AREA IT | 9718.7 | 10974.7 | 12168.8 | 18540.4 | 14494.1 | -172.4 |
| AREA NL | 5433.8 | -42.0 | 4247.2 | 6564.2 | 3432.9 | -358.1 |
| AREA PL | 3821.0 | -648.9 | 9881.1 | 8232.6 | 4681.5 | 139.1 |
| AREA PT | 1104.7 | -234.4 | 3031.5 | 2833.9 | 1218.5 | -150.7 |
| AREA SI | 937.1 | 0.0 | 369.0 | 727.4 | 551.4 | 27.3 |
| TOTAL | 65991.8 | 10296.0 | 130234.9 | 130843.9 | 75680.4 | |

Concerning the reactive power balance, is important to remark the reactive power coming from the shunt elements. Those shunt elements have been added to the system first to achieve convergence, and then to improve the reactive power margin of generation units. Some areas have required reactive power injections from capacitors, such as Italy where more than 10000 MVar had to be added. On the other hand, in other areas, such as Great Britain or Denmark, reactors to absorb reactive power have been placed.

Table XVI provides a perspective of the voltage profile of the system including the minimum and maximum voltage of each area, plus the mean voltage and the standard deviation. Figure 42 represents the distribution of system voltages.

Table XVI – System voltages report

| area | mean | std | min | max |
|---------|-------|-----|-------|-------|
| AREA AT | 384.4 | 3.2 | 378.3 | 388.9 |
| AREA BE | 385.3 | 2.3 | 380.8 | 391.2 |
| AREA CH | 386.3 | 2.6 | 382.4 | 390.1 |
| AREA CZ | 388.0 | 4.5 | 372.3 | 394.6 |
| AREA DE | 385.9 | 6.6 | 371.8 | 407.2 |
| AREA DK | 388.3 | 1.5 | 385.6 | 390.8 |
| AREA ES | 388.1 | 6.4 | 362.5 | 398.7 |
| AREA FR | 388.6 | 6.1 | 359.0 | 405.0 |
| AREA GB | 390.6 | 2.9 | 385.5 | 395.7 |
| AREA IT | 386.0 | 7.5 | 354.0 | 396.9 |
| AREA NL | 383.9 | 4.1 | 377.4 | 396.7 |
| AREA PL | 389.2 | 7.4 | 365.3 | 407.4 |
| AREA PT | 390.1 | 2.1 | 387.1 | 394.3 |
| AREA SI | 383.6 | 3.9 | 377.0 | 387.3 |
| AREA SI | 387.2 | 6.2 | 354.0 | 407.4 |

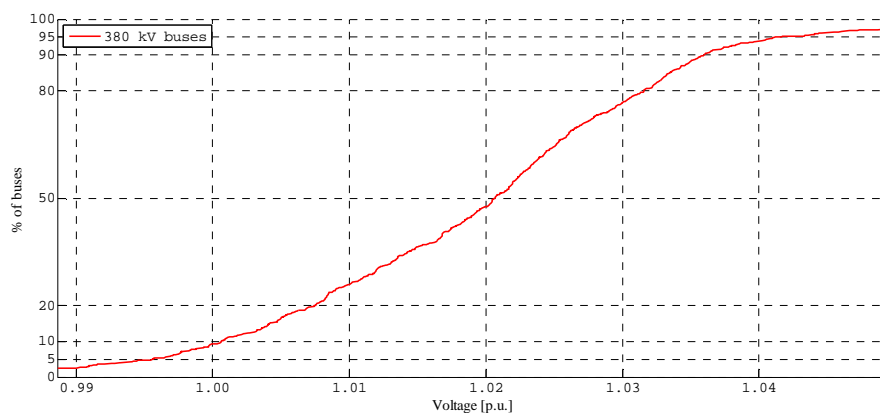


Figure 42 – Distribution of bus voltages, in pu

7.5.2. Voltages robustness

Table XVII illustrates the distance to the voltage collapse assuming two generator models (reactive power limits off and on) and two types of load models (constant reactive load and constant power factor). As it was expected, the margin to voltage collapse becomes smaller if both generator reactive power limits and constant power factor loads are assumed.

The corresponding P-V curves are shown from Figure 43 to Figure 46. P-V curves show the variation of the voltage magnitude of selected buses as the system demand increases. The voltage variation is computed and displayed until the point of voltage collapse which indicates the maximum loadability of the system. One characteristic (pilot) bus has been chosen from each area.

Table XVII – Margin to voltages collapse

| | INITIAL | FINAL (limQ OFF) | FINAL (limQ ON) |
|------------------|---------|------------------|------------------|
| Constant Q load | 371400 | 431114 (+16.1 %) | 419276 (+12.9 %) |
| Constant FP load | 371400 | 414923 (+11.7 %) | 404478 (+8.9 %) |

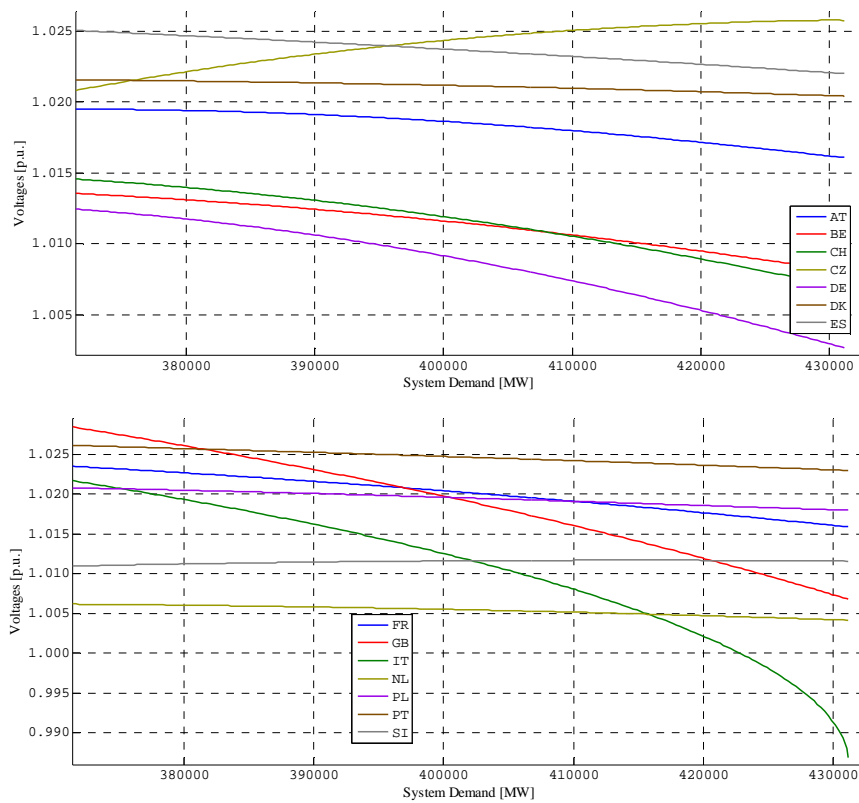


Figure 43 – Bus voltages during demand increase, without considering reactive power generation and reactive power demand variation

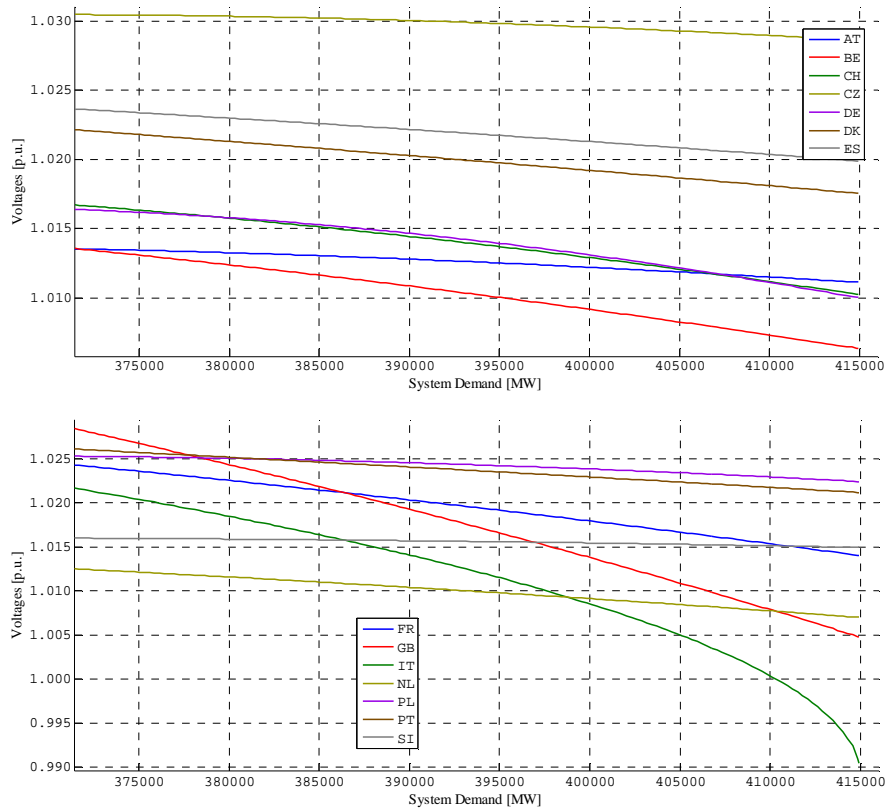


Figure 44 – Bus voltages during demand increase, without considering reactive power generation, and assuming constant power factor for demand

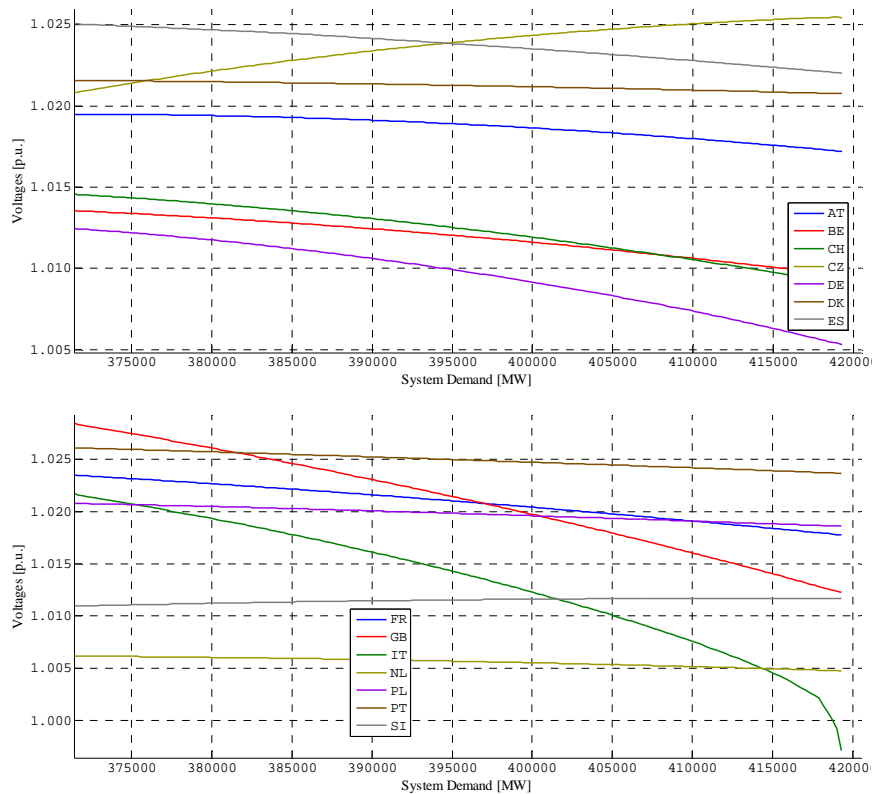


Figure 45 – Bus voltages during demand increase, considering reactive power generation and no reactive power demand variation

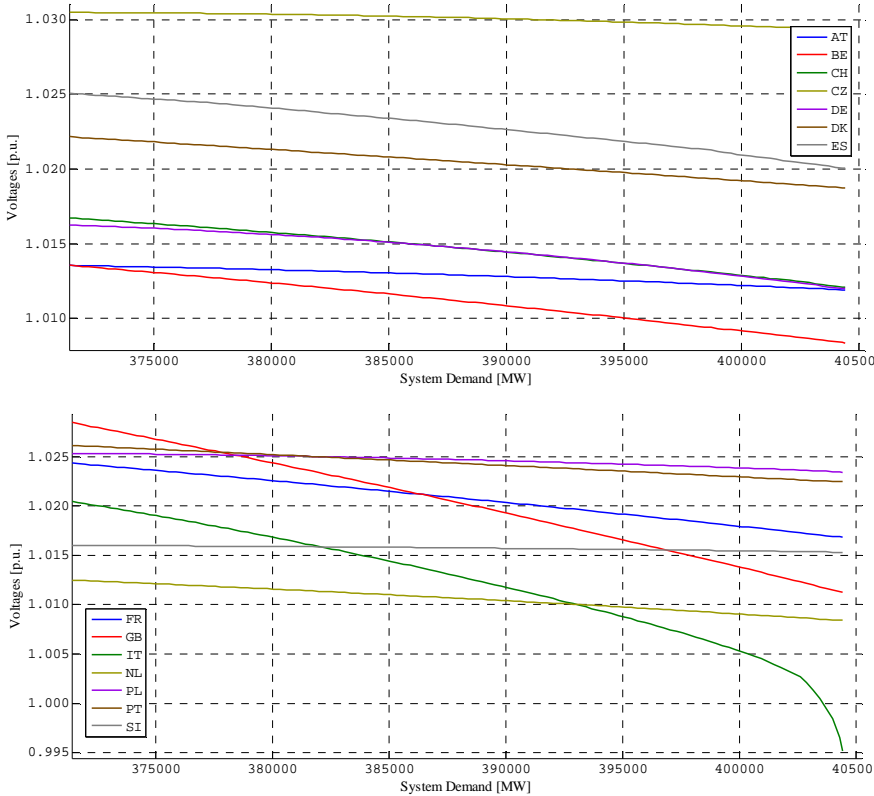


Figure 46 – Bus voltages during demand increase, considering reactive power generation, and assuming constant power factor for demand

8. Conclusions

Work Package 8 of the e-Highway2050 project [3] aims at defining a new methodology where long-term planning is formalised as an optimisation problem, and at specifying new tools. Advanced optimisation and simulation methods were investigated to tackle this complex highly combinatorial problem, taking into account the stochastic and dynamic behaviours of the system. A Monte-Carlo approach has been retained to consider the stochasticity of the problem. The problem is solved from a transmission operator perspective, with no control over generation planning. Though, several possible evolutions of the electricity sector are investigated for different scenarios. The main challenges arise from the spatial, temporal and stochastic complexities. Thus, methods to reduce the size of the grid or to choose relevant snapshots among the 8760 hours of a year have been developed.

The complete methodology has been tested on a real size test case. The studied system was based on a large part of the European system, so that it was close to the size of the European network ($\approx 5,000$ nodes). Three different energy mix scenarios were studied for three time horizons, up to 2050. Then, 900 Monte-Carlo years, i.e. consumption and production scenarios, were generated to consider the stochasticity of the problem. Hourly system simulations in copperplate were run for each year to ensure power adequacy between production and load. In the following step, overload problems were detected on the simplified initial nodal grid (around 1,000 nodes) to identify critical branches, which were used to build a zonal initial grid model (100 nodes) from the nodal one. After having selected a few snapshots among the whole set of Monte-Carlo years and a few interesting candidates for the zonal expansion, the modular development plan was calculated at the zonal level considering all time horizons and scenarios. Starting from the zonal modular development plan, a grid expansion was then performed for the first time horizon, i.e. 2030, at the nodal level. Finally, the robustness of the nodal grid architectures was checked to ensure that these grids can be operated without major voltage or stability issues.

Parallelization on 9 servers with 16 cores each was used to perform the test case. Each server corresponds to one scenario and one time horizon, thus 100 Monte-Carlo years were simulated by server. The obtained computation times and output data volumes for each module are gathered in Table XVIII. It took around 48h to run the methodology up to the nodal expansion. Some modules can still be improved to reduce the computation time and increase the number of selected snapshots. Indeed, we selected 5 snapshots among 100 years, however it would be interesting to study the impact of selecting more snapshots on the expansion results. We propose several recommendations to increase the efficiency of the prototype, such as looking at different languages or taking advantage of MILP solver improvements. The total data volume generated to simulate 900 Monte-Carlo years on a European size network reached 6TB, which is quite significant and should be considered in the resources assessment.

Thus, the proposed methodology is feasible, although further work is still needed to improve its efficiency and sensitivity studies should be performed to tune some input parameters, such as the snapshot selection criteria. Taking advantage of the parallelization of some modules over several servers, it should be possible to run a real long-term case study on the full European grid within a reasonable time (less than 48h). This kind of study could be performed once a year and help the planner decide which reinforcements should be planned. On the shorter term, parts of the method could be implemented in existing tool to improve current practices. The automation of some modules could also be used to perform sensitivity studies on input parameters and test the impact of different scenario assumptions on transmission grid development.

The main outputs of Work Package 8 and raised issues are tackled in deliverable 8.7 on “Recommendations about critical aspects in long-term planning methodologies” [24].

Table XVIII – Computation times and output data volumes

| | Average computation time for 1 year | Total computation time | Output data volumes |
|---|--|-------------------------------|----------------------------|
| Time Series generation | 6min | 30h | 2160 GB |
| Hydro scheduling | 2min | | |
| Adequacy (total time for the 52 weekly MILP problems) | 2h 37min | | |
| Disaggregation | 13min | | |
| Nodal DCOPFs (total time for the 8760 hourly linear problems) | 1h 53min | | 2520 GB |
| Calculation of indicators | 5min | | |
| Network reduction (from 1000 nodes to 100 zones) | - | 1min | - |
| Zonal DCOPFs (total time for the 8760 hourly linear problems) | 40min | 4h | 990 GB |
| Zonal price differences calculation (average, min, max, standard deviation over the system) | 24min | 2h 20min | 315 GB |
| Snapshot selection (5 snapshots per scenario/horizon) | - | 30min | - |
| Candidate selection | - | 2h 27min | - |
| Zonal TEP optimization with 45 snapshots and 56 candidates | - | 2h | - |
| Nodal expansion | - | 20min | - |
| TOTAL | - | 41h 40min | 6 TB |

REFERENCES

- [1] AMPL Optimization, <http://ampl.com>
- [2] Bahiense, L., Oliveira, G. C., Pereira, M., & Granville, S. (2001). A mixed integer disjunctive model for transmission network expansion. *Power Systems, IEEE Transactions on*, 16(3), 560-565.
- [3] e-Highway2050, <http://www.e-highway2050.eu>
- [4] e-Highway2050 (2014). D2.1: Data sets of scenarios for 2050. Available at: <http://www.e-highway2050.eu/results>
- [5] e-Highway2050 (2014). D3.1: Technology assessment from 2030 to 2050. Available at: <http://www.e-highway2050.eu/results>
- [6] e-Highway2050 (2015). D8.2a: Enhanced methodology for the computation of Demand and Generation scenarios. Available at: <http://www.e-highway2050.eu/results>
- [7] e-Highway2050 (2015). D8.3a: Enhanced methodology to define optimal grid architectures for 2050. Available at: <http://www.e-highway2050.eu/results>
- [8] e-Highway2050 (2015). D8.4a: Enhanced methodology to define the optimal modular plan. Available at: <http://www.e-highway2050.eu/results>
- [9] e-Highway2050 (2015). D8.5a: Enhanced methodology to assess robustness of a grid architecture. Available at: <http://www.e-highway2050.eu/results>
- [10] e-Highway2050 (2015). D8.5b: Prototype to assess robustness of a grid architecture. Available at: <http://www.e-highway2050.eu/results>
- [11] ENTSO-E (2013). ENTSO-E Memo 2012. Available at: https://www.entsoe.eu/fileadmin/user_upload/_library/publications/entsoe/Memo/2012_ENTSO-E_Memo.pdf
- [12] FICO Xpress Optimization Suite, FICO, <http://www.fico.com/en/products/fico-xpress-optimization-suite/>
- [13] Kaufman, L., & Rousseeuw, P.J. (1987). Clustering by means of Medoids. In Y. Dodge (Ed.). *Statistical Data Analysis Based on L_1 -Norm and Related Methods*, pp. 405-416. New-York.
- [14] Kaufman, L., & Rousseeuw, P.J. (1990). Clustering Large Applications (Program CLARA). *Finding Groups in Data: An Introduction to Cluster Analysis*. John Wiley & Sons, New-York.
- [15] Li, Y., & McCalley, J.D. (2014). Design of A High Capacity Inter-Regional Transmission Overlay for the U.S. *Power Systems, IEEE Transactions on*, 30(1), 513-521.
- [16] Lumbreras, S., Ramos, A., & Sánchez, P. (2014). Automatic selection of candidate investments for transmission expansion planning. *International Journal of Electrical Power & Energy Systems*, 59(0), 130-140.
- [17] Lumbreras, S., & Ramos, A. (2013). Transmission expansion planning using an efficient version of benders' decomposition. A case study. *PowerTech (POWERTECH), 2013 IEEE Grenoble*, pp. 1-7.
- [18] McCalley, J. D., Aliprantis, D., Dobson, A., Li, Y., & Villegas, H. (2013). High capacity interregional transmission system design. *Report for RTE*.

- [19] Munoz, F.D., Hobbs, B.F., & Kasina, S. (2012). Efficient proactive transmission planning to accommodate renewables. *Power and Energy Society General Meeting, 2012 IEEE*, pp. 1-7.
- [20] Ng, R., & Han, J. (2002). CLARANS: A Method for Clustering Objects for Spatial Data Mining. *Knowledge and Data Engineering, IEEE Transactions on*, 14(5), 1003-1016.
- [21] Renedo, J., García-Cerrada, A., Sanz, S., Zamora, J. L., Rouco, L., Fernández, C. & García-González, P. (2015). Entregable E2.3: Estudio de la aplicación de la tecnología HVDCVSC multi-terminal y sus aplicaciones. *ESP-LIDER: Electrónica de Potencia en el Sistema Eléctrico para la Integración de Energías Renovables*. Ref IPT-2011-0844-920000., Tech. Rep.
- [22] Shi, D. & Tylavsky, D. J. (2012). An improved bus aggregation technique for generating network equivalents. *Power and Energy Society General Meeting, 2012 IEEE*, pp. 1-8.
- [23] Wilkinson, J. H. (1965). The Algebraic Eigenvalue Problem. *Clarendon Press, Oxford*.
- [24] e-Highway2050 (2015). D8.7: Recommendations about critical aspects in long-term planning methodologies. Available at: <http://www.e-highway2050.eu/results>

APPENDIX

The data format for AC and AC/DC load flow input files including VSC-HVDC links is as follows.

- First line:
System MVA base.
- For every AC bus:
AC bus number, Bus type (= 1 load bus; = 2 generation bus; = 3 swing bus), PG, QG, PL, QL, GS, BS, VM, VA.
- For every AC branch:
From AC bus number, To AC bus number, Circuit number, Branch type (= 0 transmission line; = 1 transformer), R, X, B, TAP, PHASE, GI, BI, GJ, BJ
- For every AC/DC VSC converter:
Converter number, DC bus number, AC bus number, Active power control (= 1 DC power control; = 2 DC voltage control), Reactive power control (= 1 Reactive power control; = 2 AC voltage control), VM, VA, PCONV, QCONV, RT, XT, BF, RC, XC, A, B, CRECT, CINV
- For every DC bus:
DC bus number, DC grid number, VDC, PDC, GDC, CDC
- For every DC branch:
From DC bus number, To DC bus number, RDC, LDC, CCC, PDCIJ, PDCJI

The data format for dynamic input files is as follows:

- Salient pole generator model:
Bus number, "GENSAL", MBASE, H, D, TPD0, TPPD0, TPQ0, TPPQ0, XD, XQ, XPD, XPPD, XL, S1, S2, R
- Round generator model:
Bus number, "GENROU", MBASE, H, D, TPD0, TPPD0, TPQ0, TPPQ0, XD, XQ, XPD, XPD, XPPD, XL, S1, S2, R
- RES model
Bus number, "GNWTBL", MBASE, R, TG, KV, TV, TD, TQ
- EXAC3 excitation model
Bus number, "EXAC3", TR, TB, TC, KA, TA, TE, KR, KF, TF, KN, EFDN, KC, KD, KE, E1, SE1, E2, SE2
- EXAC1 excitation model
Bus number, "EXAC1", TR, TB, TC, KA, TA, TE, KF, TF, KC, KD, KE, E1, SE1, E2, SE2
- ESST4B excitation model
Bus number, "ESST4B", TR, KPR, KIR, TA, KPM, KIM, KG, KP, KI, KC, XL, THETAP

- ST6B excitation model
Bus number, "ST6B", TR, KPA, KIA, KDA, TDA, KFF, KM, KG, TG
- ST6B excitation model
Bus number, "ST6B", TR, KPA, KIA, KDA, TDA, KFF, KM, KG, TG
- IEEEG1 governor model
Bus number, "GOV1", K, T1, T2, T3, T4, T5, T6, T7, K1, K3, K5, K7
- GGOV1 governor model
Bus number, "GGOV1", TBASE, R, TPELEC, KPGOV, KIGOV, KDGOV, TDGOV, TACT, KTURB, TB, TC, TENG, DM
- GAST2A governor model
Bus number, "GAST2A", W, X, Y, Z, TCD, TRATE, T, ECR, K3, A, B, C, TF, KF, AF2, BF2, CF2
- HYGOV governor model
Bus number, "HYGOV", R, RT, TR, TF, TG, TW, AT, DTURB, QNL
- DC grid model
DC grid number, "DCGRID", DCGRIDID
- AC/DC converter model
AC bus number, "SVSCOM", Circuit number, VSCBASE, VACBASE, VDCBASE, DCGRIDID, Number of poles, Active power control (= 1 DC power control; = 2 DC voltage control), Reactive power control (= 1 Reactive power control; = 2 AC voltage control), TD, TQ, KD1P, KD1I, KD2P, KD2I, KQ1P, KQ1I, KQ2P, KQ2I, A, B, CRECT, CINV, RS, XS